Dynamic properties of well-graded sand with silt

Nuraiym Sagadi, B.eng

Submitted in fulfillment of the requirements
for the degree of Master of Science
in Civil & Environmental Engineering

School of Engineering and Digital Sciences
Department of Civil & Environmental Engineering
Nazarbayev University

53 Kabanbay Batyr Avenue,
Astana, Kazakhstan, 010000

Supervisor: Sung-Woo Moon
Co-supervisor: Jong Kim

2nd May

Abstract

Designing robust geotechnical buildings and foundations requires understanding the dynamic qualities of soils, especially how they behave during cyclic or dynamic loading circumstances, such as those caused by seismic events or construction operations. Using the Resonant Column and Cyclic Torsional Shear (CTS) tests, this study examines silty and well-graded sand soils from Astana, Kazakhstan, to describe their dynamic behavior under different confining pressures (σ_c). Despite the relatively low level of seismic activity in Astana, aftershocks from remote earthquakes emphasize how crucial it is to comprehend the seismic risks unique to a certain location. This study offers site-specific material damping ratio (D) and shear modulus diminution (G) curves, which are crucial for assessing seismic risks and catastrophe mitigation. With its real-world uses in foundation construction, urban planning, and seismic risk mitigation, these findings fill important gaps in the dynamic characterization of well-graded sand with silt and help create safer and more durable buildings in earthquake-prone areas.

Keywords: dynamic soil properties, resonant column, cyclic torsional shear, shear modulus, well-graded sand with silt

Table of Contents

Abstract---- **1**
Chapter 1. Introduction---- **6**
1.1 Overview---- 6
1.2 Thesis statement---- 6
1.3 Aim---- 7
1.4 Objectives---- 7
1.5 Methodologies and techniques---- 7
1.6 Thesis structure---- 8
Chapter 2. Literature review---- **9**
2.1. Geology and Seismicity of the country---- 9
2.1.1. Seismicity of Kazakhstan---- 9
2.2. Small strain nonlinearity---- 12
2.3. Dynamic Soil properties---- 14
2.3.1. Shear Modulus---- 15
2.3.2. Damping Ratio---- 15
2.3.3. Normalized shear modulus reduction curve---- 18
2.4. Application of dynamic soil characteristics---- 21
Chapter 3. Methodology---- **22**
3.1. Methods to determine dynamic soil properties---- 22
3.1.1. Field tests---- 22
3.1.2. Laboratory tests---- 22
3.2. Device - Resonant Column Apparatus---- 24
3.3. Sample preparation---- 26
Chapter 4. Testing procedure---- **27**
4.1. Resonant Column Test---- 30
4.1.1. Shear modulus establishment---- 33
4.1.2. Damping ratio establishment---- 34
4.2. Cyclic Torsional Shear Test (CTS)---- 35
4.3 Calibration---- 35
Chapter 5. Physical Properties of the Soil---- **38**
Chapter 6. Test Results---- **42**
6.1. Calibration results---- 42
6.2. Resonant Column (RC) Test---- 44
6.2.1. Shear modulus vs. shear strain (G vs. γ)---- 45
6.2.2. Damping ratio vs. shear strain (D vs. γ)---- 46
6.3. Cyclic Torsional Shear Testing---- 47

6.3.1. Shear modulus vs. shear strain (G vs. γ)---------- 47
6.3.2. Damping ratio vs. shear strain (D vs. γ)---------- 48
6.3.3. Impacts of Shearing Strain---------- 49
6.3.4. Impacts of Loading cycles---------- 51
6.4. Normalized shear modulus (G/Gmax vs. γ)---------- 53
6.5. Damping ratio (D vs. γ)---------- 54
Chapter 7. Conclusion----------56
References----------58

List of Figures

Figure 2.1. (a)Almaty's tectonic setting, (b)RGB Landsat image (Amey et al.,2021) 10
Figure 2.2. (a) Almaty with epicenters of the Verny and Kemin earthquakes; (b) present-day Almaty, historic Verny and active faults (c) microseismic intensity from the Kemin event with liquefaction and ground failures (Alshembari et al., 2020) 11
Figure 2.3. Almaty's ground failure (Kemin earthquake) 11
Figure 2.4. G/Gmax vs. shear strain (Wong et al., 2021) 12
Figure 2.5. (a) P-wave, (b) S-wave, (c) Rayleigh wave and (d) Love wave (Kramer, 1996) 13
Figure 2.6. Hysteresis loop during a single loading cycle 16
Figure 2.7. Damping ratio vs. shear strain for clays and sand (Vucetic & Dobry, 1991) 18
Figure 2.8. Cyclic stiffness degradation on sand and clay (PI=0) (Vucetic and Dobry, 1991) 19
Figure 2.9 - a. Maximal fitting curves for modulus degradation (Oztoprak & Bolton, 2013) 20
Figure 2.9 - b. Maximal fitting curves for modulus degradation (Oztoprak & Bolton, 2013) 20
Figure 3.1. RC apparatus with its elements (Sakshi & Sebastian 2023) 25
Figure 4.1. Configuring a test to run RCA tests (Dutta, 2015) 29
Figure 4.2. Electromagnetic system of RCA (GDS Resonant Column, 2010) 31
Figure 4.3. Torsional and flexural excitation (GDS Resonant Column, 2010) 31
Figure 4.4. Schematic diagram of RCA system (GDS Resonant Column, 2010) 32
Figure 4.5. Schematic diagram of RCA system 33
Figure 4.6. Free vibration decay curve (GDS Resonant Column, 2010) 34
Figure 4.7. Calibration bars and weights 36
Figure 4.8. Excel spreadsheet for the calibration calculation 36
Figure 4.9. Example of the calibration **(** I_{am} vs. w/2) 37
Figure 5.1. Testing site in Astana, Kazakhstan 39
Figure 5.2. Well-graded sand with silt in Astana, Kazakhstan (Sagidullina et al., 2025) 39
Figure 5.3. OMC and MDD of well-graded sand with silt 40
Figure 5.4.(a) Particle size distribution curve;
(b) SEM image of the well-graded sand with silt 40
Figure 6.1. Calibration results for aluminum bars with varying diameters using added masses 42
Figure 6.2. A typical illustration of damping ratio testing 44
Figure 6.3. A typical illustration of the resonance frequency for a particular shear strain magnitude 45
Figure 6.4. G vs. γ for different σ_c (for RC tests) 46
Figure 6.5. D vs. γ for different σ_c (for RC tests) 47
Figure 6.6. G vs. γ for different σ_c (for CTS tests) 48
Figure 6.7. D vs. γ for different σc (for CTS tests) 49
Figure 6.8. Hysteretic response of the sample at different loading cycles 50
Figure 6.9. Hysteretic response of the sample at different voltages 52
Figure 6.10. G/Gmax vs. γ 53
Figure 6.11. D vs. γ 55

List of Tables

TABLE 2-1. Factors for testing soil's dynamic characteristics (Seed and Idris,1970) 17
TABLE 2-2. Constants of Equation (2.7) (Szilvágyi, 2018) 21
TABLE 3-1. Measurement methods of dynamic properties (Kumar et al.,2013) 23
TABLE 5-1. Physical characteristics of the soil specimens 41
TABLE 6-1. Calibration results 43
TABLE 6-2. Computed values for determining the shear modulus 44

Chapter 1. Introduction

1.1 Overview

This study presents the work on dynamic soil properties in Kazakhstan, providing an extensive literature review, the methodology for their determination, and an overview of Kazakhstan's seismicity. Moreover, it explores the primary research concepts and presents the thesis findings.

Sustaining the security and rigidity of foundations and various buildings requires understanding how soil behaves under different stress scenarios, such as during construction or earthquakes. Road distortions, building tilting, and bridge collapses can come from soil liquefaction, a phenomenon that weakens the soil and compromises the strength of structures (Moon et al., 2024). This calls for a deep comprehension of dynamic soil features, which is crucial in geological and architectural domains such as probabilistic seismic hazard assessment (PSHA) and foundation construction (Paiyz et al., 2024). Dynamic soil properties are the study of the dynamic behavior of soil structures under diverse dynamic and cyclic loading scenarios, such as seismic activities. Shear modulus and damping ratio are two examples of dynamic soil characteristics. They fundamentally control how soils respond to dynamic loads. The shear modulus describes the soil stiffness, while the damping ratio shows how much energy the soil dissipates. The Resonant Column Apparatus (RCA), a specific testing methodology well known for its effectiveness in assessing soil behavior at small strain levels, is used in this investigation. This equipment will obtain the shear modulus, damping ratio, and normalized shear modulus curve. All of the measurements and data analysis processes are described in the thesis.

1.2 Thesis statement

Dynamic soil properties are crucial for determining how soil behaves under diverse loading circumstances, such as earthquakes or building operations, to guarantee the security and stability of foundations and other types of structures. Understanding these properties is of utmost importance in the realm of engineering and geotechnical applications, including seismic hazard assessment, foundation design, and soil-structure interaction analysis. To investigate these

dynamic characteristics of soil within the very small to intermediate range of strains, the resonant column apparatus (RCA) test methodology is applied.

1.3 Aim

This study aims to fill the critical knowledge gap by precisely investigating well-graded sand with silt using advanced soil techniques with the Resonant Column Apparatus to test for small-to-intermediate strain range. The ultimate goal is to estimate the dynamic properties of Kazakhstan's soil, enabling the creation of models for modulus reduction and material damping ratios and thereby enhancing our preparedness for seismic events in this high-risk region.

1.4 Objectives

The main objectives of the research are written below:

1. Comprehensive literature review on the dynamic soil properties;
2. Calibration of Resonant Column Apparatus to conduct future tests;
3. To carry out resonant column and cyclic torsional shear examinations on well-graded sand with silt;
4. To ascertain the dynamic soil properties of well-graded sand with silt using RCA;
5. To conduct the resonant column test and cyclic torsional shear test;
6. To analyze the data for different confining pressures;
7. To derive the Damping vs. Shear strain, Shear modulus vs. Shear strain, and Normalized Shear Modulus curve;
8. Conclude the results.

1.5 Methodologies and techniques

The soil samples from Astana's construction site will be used for this thesis work. They will be tested using a Resonant Column Apparatus manufactured by GDS Instruments to analyze the dynamic soil properties. Prior to conducting resonant column (RC) test, damping, and cyclic torsional shear (CTS) tests, the soil samples will undergo the saturation and consolidation phase to replicate the field conditions. For saturation, cell and back pressure will gradually increase until it reaches Skempton's B-Value of 0.95. After that, consolidation will be conducted at confining pressures of 50,100,150 and 200kPa. The required data for dynamic properties will

then be derived using the GDSRCA software. The shear modulus, damping ratio, and normalized shear modulus graphs at different strain values will be obtained and analyzed for future interpretation.

1.6 Thesis structure

Overall, the thesis work will contain seven chapters. It will begin with a literature review in Chapter 2, covering the key concepts of dynamic soil properties and their significance in geotechnical engineering. The chapter will also discuss the seismicity and geology of Kazakhstan, followed by a detailed description of the shear modulus, damping ratio, and the normalized shear modulus curve. Additionally, the importance of these parameters in soil behavior analysis and seismic site response studies will be highlighted. In Chapter 3, the research methodology will be outlined, detailing the field and laboratory testing techniques used to determine dynamic soil properties. The chapter will describe the Resonant Column Apparatus, its working principles, and the sample preparation process. These details will establish the foundation for the experimental procedures. Chapter 4 will focus on the testing procedure, providing a step-by-step explanation of the resonant column, damping, and cyclic torsional shear tests. This section will also cover equipment calibration, which is crucial for obtaining accurate and reliable data. In Chapter 5, the site characterization will be presented, and the physical and mechanical properties of the tested soil samples will be analyzed. This information will help correlate laboratory results with field conditions, ensuring a comprehensive understanding of the studied materials. Chapter 6 will present the experimental results, discussing the outcomes of the calibration, resonant column test, cyclic torsional shear test, and normalized shear modulus analysis. The obtained data will be analyzed to assess soil behavior under different confining pressures, providing insights into its dynamic response. Finally, Chapter 7 will conclude the thesis by summarizing key findings, discussing their implications, and proposing future research directions.

Chapter 2. Literature review

2.1. Geology and Seismicity of the country

2.1.1. Seismicity of Kazakhstan

The Tien Shan mountain region in Central Asia, despite being located 1000-1500 kilometers north of the Indian and Eurasian tectonic plate collision, is responsible for about half of the tectonic movement in the area (Amey et al., 2021). Major faults in this region may stay dormant for extended periods but tend to rupture during significant seismic events. Concealed, smaller faults branching from the main ones may exist, presenting an unidentified risk to cities near the Tien Shan mountain range.

In Kazakhstan, approximately 42.9% of the land is prone to earthquakes (Silacheva et al., 2018). This area encompasses over 400 towns and cities, including Almaty, the country's primary economic and cultural hub, hosting over 7 million people and more than 40% of the nation's industrial capacity. Historical records show severe earthquakes in the 19th and early 20th centuries, like the Belovodskoe (Ms 6.9), 1887 Verny (Ms 7.3), 1889 Chilik (Ms 8.3), and 1911 Chon-Kemin (Ms 8.2) earthquakes (Henni, 1998 and Bondár, 2011). Figure 2.2-a presents one of the two major earthquakes in Kazakhstan - Verny and Kemin. Figure 2.2-b shows Almaty's urban area along with epicenter locations, where the gray box represents the historic Verny settlement and thin black lines mark active faults. Figure (c) depicts the macroseismic intensity distribution from the Kemin event in the Verny region, with areas of ground failures and liquefaction highlighted by black lines (Alshembari et al., 2020). According to the sources at that period, every building was somewhat damaged (Bogdanovic, 1911; Bogdanovich et al., 1914). Of the 390 fatalities caused by this earthquake, 44 occurred in Verny (Almaty) alone. Surprisingly, this earthquake caused substantial ground collapse and soil distortion in Verny, which is around 40 kilometers from the epicenter (Alshembari et. al, 2020). This was especially true for the loam and sandy soils. In many locations, the cracks were 1 m wide and 5 m deep (Figure 2.3). However, recent records do not document significant earthquakes (Ms > 7) due to extended seismic inactivity. Due to prolonged dormancy, the Institute of Seismology of Kazakhstan has

raised concerns about the potential for significant earthquakes in the Almaty area (Tectonic structures, 2023).

In Figure 2.1.-a, the geological setting of Almaty in the northern Tien Shan is shown, with GPS velocities related to stable Eurasia and 95% confidence ellipses (Amey et al., 2021). Historical earthquake epicenters are marked in white, and active faults are displayed in red and light orange. The border between Kyrgyzstan and Kazakhstan is indicated in yellow. In Figure 2.1-b, an RGB Landsat image of Almaty is presented, featuring dynamic faults in light orange and the mapped crack. Despite Astana's low seismic activity risk, people in the city experienced aftershocks in January from earthquakes that occurred 1600–3000 kilometers distant in China and Kyrgyzstan.

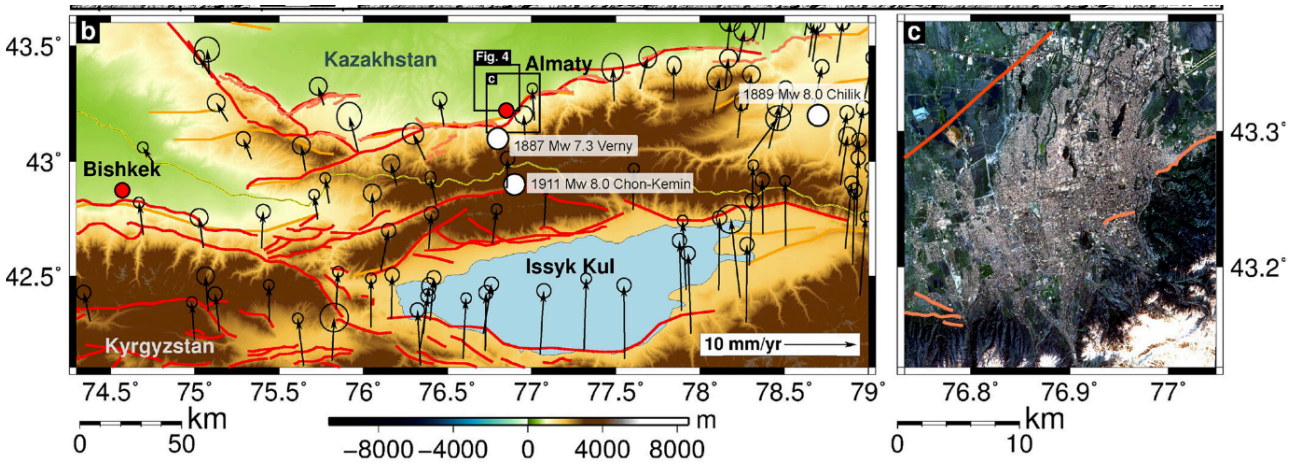

Figure 2.1. (a) Almaty's tectonic setting, (b) RGB (red, green, blue) Landsat image (Amey et al., 2021)

Over the last 50 years, Kazakhstan's seismic design regulatory framework has undergone substantial evolution. Initially, it was founded on studies conducted during the Soviet era. Since its initial release in 1998, the first extensive building norms (SNiP), have undergone many changes to take into account developments in earthquake engineering and findings from worldwide study (Zhanabayeva et al., 2023).

Recently, Kazakhstan shifted to implementing European seismic design standards, spurred on by the "100 steps" strategy to improve building effectiveness and security

(Zhanabayeva et al., 2023). As part of this shift, national standards will incorporate Eurocode concepts, allowing for the unification of safety and sustainability.

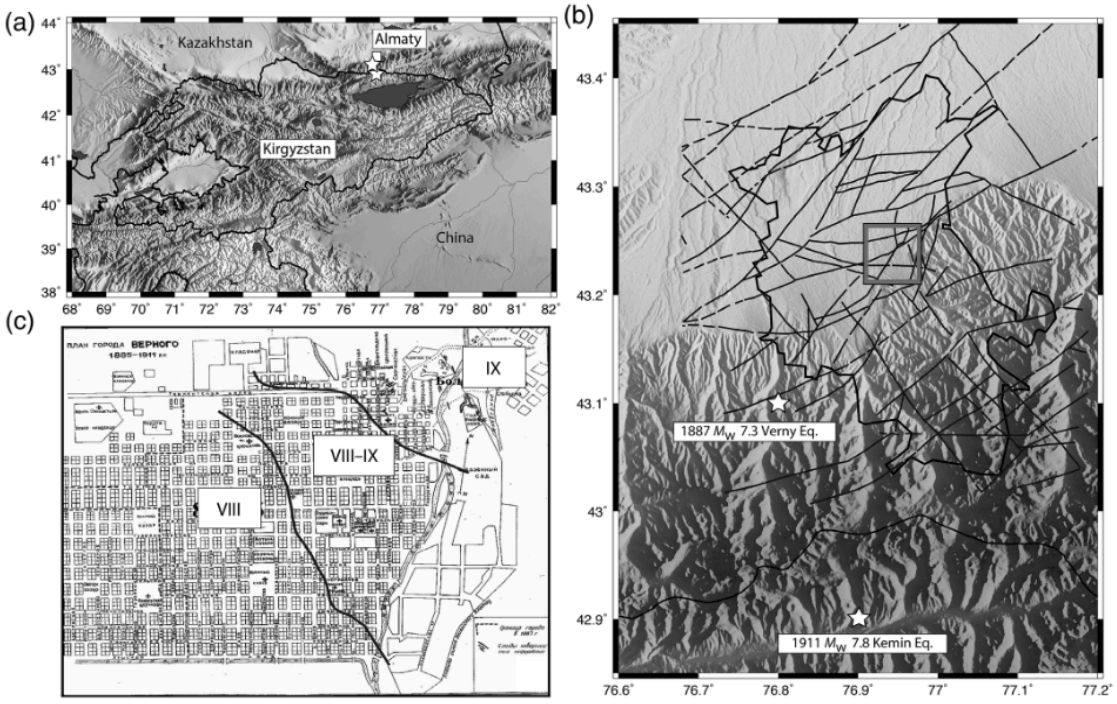

Figure 2.2. (a) Almaty with epicenters of the Verny and Kemin earthquakes; (b) present-day Almaty, historic Verny and active faults (c) microseismic intensity from the Kemin event with liquefaction and ground failures (Alshembari et al., 2020)

Figure 2.3. Almaty's ground failure (Kemin earthquake)

Notwithstanding, obstacles persist in executing these guidelines because of variations in design approaches, insufficient suitable materials, and technological circumstances. The SP RK 2.03-3-2017* record, which blends traditional local laws with Eurocode criteria, is one attempt to solve these issues. By assuring the security and worldwide viability of Kazakhstan's building sector, this combination seeks to make European standards more applicable there (Zhanabayeva et al., 2023).

In Kazakhstan, there are a variety of buildings using different construction materials and seismic-resistant techniques. However, pre-1990s residential structures lack seismic resilience due to the absence of seismic design standards (Rashid et al., 2023 and 2024). Moreover, the dynamic soil qualities of Kazakhstan have not been well studied so far, even with sophisticated testing techniques such as the Resonant Column Apparatus (RCA) test. With the area not experiencing a significant earthquake for over a century, there has been limited public awareness of seismic risk. Government authorities must assess seismic hazards and develop a strategy to reduce the risk of a catastrophic event. For that, it is important to measure the dynamic properties of the soil.

2.2. Small strain nonlinearity

Strain range categorization, stress-strain action, degradation category, and pore pressure condition are displayed by G/G_{max} vs. shear strain in Figure 2.4.

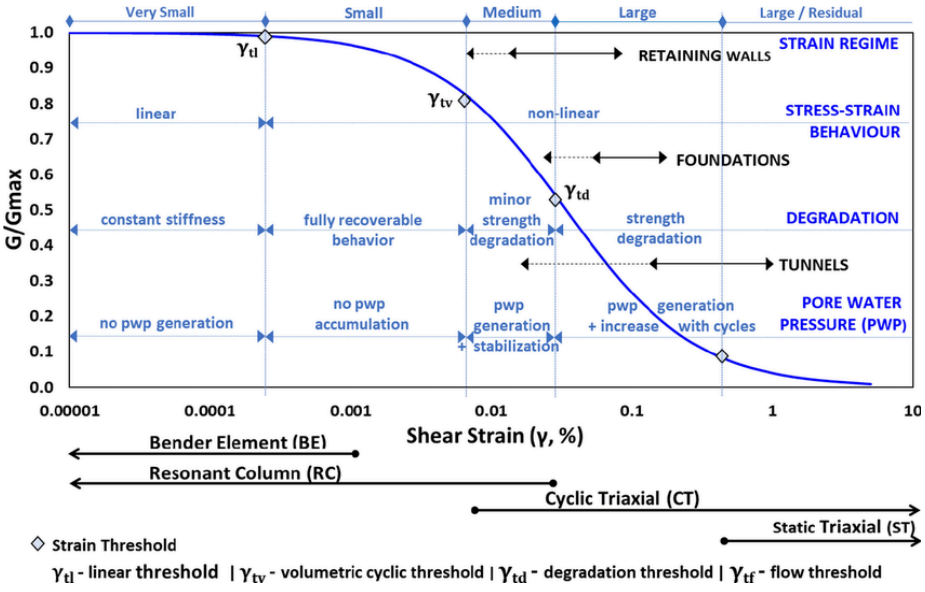

Figure 2.4. G/G_{max} vs. shear strain (Wong et al., 2021)

The normal strain values associated with various soil behaviors and assessment limits for lab instruments are also given. For the geological simulation in earthquakes, railroads, and settlements, intergranular slippage causes soil stiffness to decrease as strain increases, as shown in Figure 2.4. Soil exhibits linear behavior at extremely low stresses (10^{-6} to 10^{-4} %), although G/G_{max} steadily decreases as strain grows. Shear modulus momentarily returns as the load flips during cyclic loading, but additional stress causes stiffness degradation to occur again.

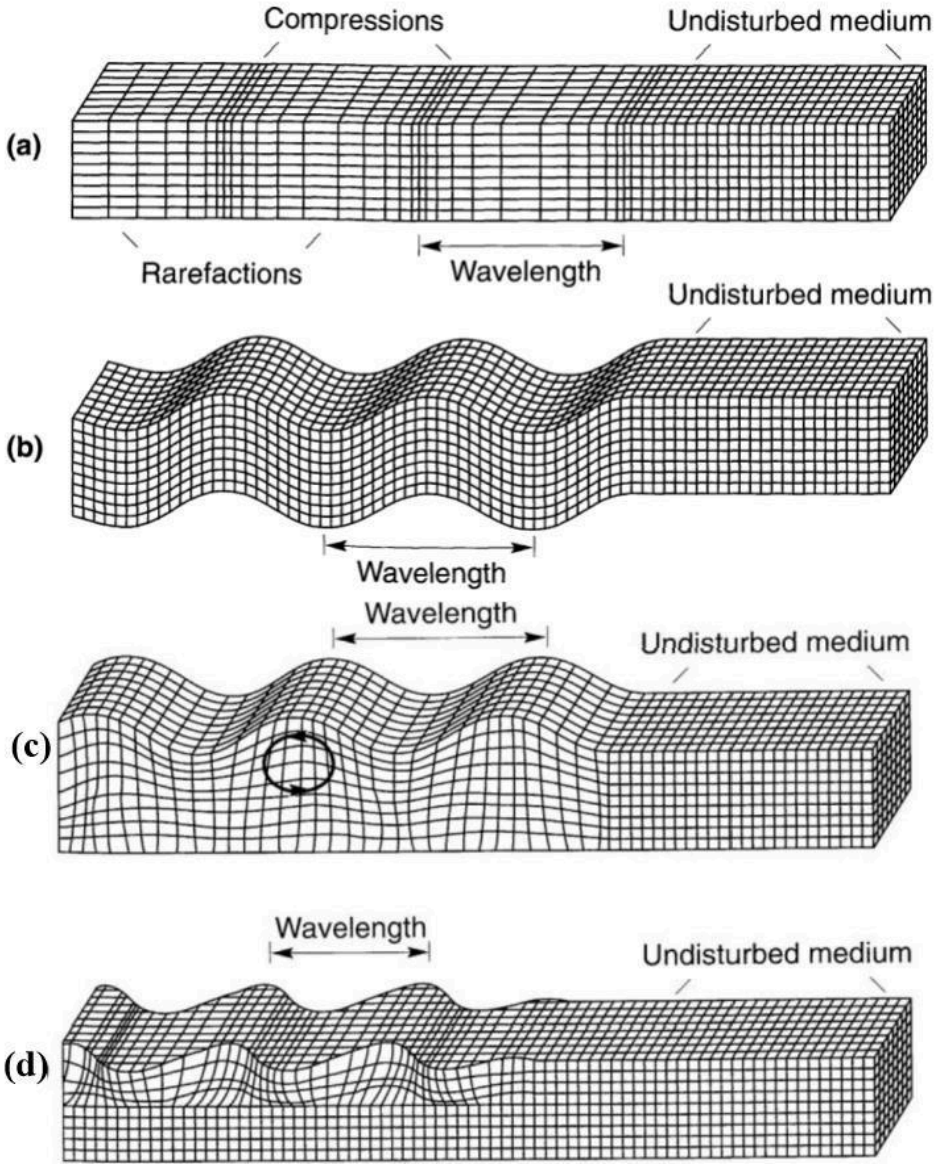

Figure 2.5. (a) P-wave, (b) S-wave, (c) Rayleigh wave, and (d) Love wave (Kramer, 1996)

This extremely low strain level is common in waves and other vibrations caused by earthquakes. It is commonly recognized that the energy produced during an earthquake causes seismic waves, as shown in Figure 2.5, which spread throughout the quantity of earth and rock along with the surface of the ground. From that, S-waves are most critical because they engage cruelly with buildings and transport much energy. Since shear waves go from harder to softer layers, they refract at level borders. They frequently arrive at the outermost layer as horizontally polarized, almost vertical waves, which cause horizontal shear stresses in the soil (Szilvagyi, 2018). For this reason, shear modulus and shear strain levels are commonly used to characterize small strain nonlinearity.

2.3. Dynamic Soil properties

Dynamic soil properties, or mechanical characteristics of the soil, are the general terms used to describe the response of the soil under dynamic loading conditions. Understanding and designing foundations, substructures, soil retaining structures, and other soil-based constructions like earth and rock fill dams to withstand earthquakes relies heavily on knowing the dynamic properties of the soil (Bharat, 2011). To ascertain the dynamic properties of the soil, it is essential to consider the attributes of these solid particles and the interplay among soil, water, and air. Foundation and retaining structure problems resulting from dynamic loads are typically classified as exhibiting either a low or high strain amplitude response (Sitharam et al., 2021). Structures can endure significant strain levels during seismic events. The following are the main soil characteristics needed to understand how a structure responds to dynamic loads (Das and Luo, 2016):

1. Dynamic Young's and shear moduli (E and G, respectively): affected by confining pressure and rate of strain;
2. Poisson's ratio (μ): for cohesive soils - range between 0.25-0.35, for cohesionless soils - 0.35-0.45;
3. Damping ratio (D): determined by the dynamic testings;
4. Variables of liquefaction (e.g. cyclic shear strength);

Moreover, it is necessary to study the response received following various loading cases to ascertain these qualities. Hysteresis response is observed when cyclic loading is applied to a

typical soil. Two characteristics that characterize the general form of the hysteresis loop or the loop's route can be used to define the cyclic loading of common soil. According to Luna and Jadi (2000), these factors include the damping ratio, shear modulus, and the backbone curve. Different-sized loops will form when the strain intensity of cyclic loading is changed (Shankar et al., 2013).

2.3.1. Shear Modulus

The modulus of shear (G) is often used to express soil stiffness. As seen in Figure 2.6, G is often referred to as the slant of a secant line connecting the highest and lowest ends on a hysteresis loop at a certain shear strain. The plot of shear stress (τ) vs. shear strain (γ) will generate a hysteresis similar to or equal to the loop, illustrated in Figure 2.6, when the soil sample is exposed to symmetrical cyclic loading in cyclic torsional shear. The greatest shear modulus at low strain levels may be computed directly from the graph's backbone curve, whose key feature is inclination (Hoque, 2016). The tangent G may be used to explain the soil's stiffness at any stage of the loading process, which determines the loop's inclination. The secant G can be used to estimate the average value of the tangent G throughout a load cycle, but it fluctuates throughout the loop. Thus, explain the hysteresis loop's overall inclination.

$$G_{sec} = \frac{\tau_{pp}}{\gamma_{pp}} \qquad (2.1)$$

Where, G_{sec} is the secant shear modulus (average of soil stiffness), τ_{pp} is shear stress, γ_{pp} is the shear strain. Figure 2.6 depicts how G_{sec} changes in proportion to the amplitude of γ_{pp}. It is large for small strain values and becomes less for higher strain values. Several researchers have verified that the relative density, confining pressure, and the shear strain ratio significantly impact the shear modulus. For that reason, in this thesis, the impact of these factors is studied and analyzed.

2.3.2. Damping Ratio

Although Moayerian (2012) defined material damping as the ratio between system damping and critical damping (no oscillation), Kramer (1996) said that material damping indicates the loss of strain energy under cyclic loading, even at very low strain rates. The soil element's capacity to attenuate dynamic forces increases as its stiffness decreases with strain

amplitude. This is because friction, heat, or plastic yielding causes the soil to lose energy. According to Abu (2011), the damping coefficient (D) equates to the area of the hysteretic loop. It is clear from Figure 2.6 that the amount of the strain that constitutes the loop of hysteresis will affect each of these features; therefore, both D and shear modulus must be calculated as proportions to the generated strain.

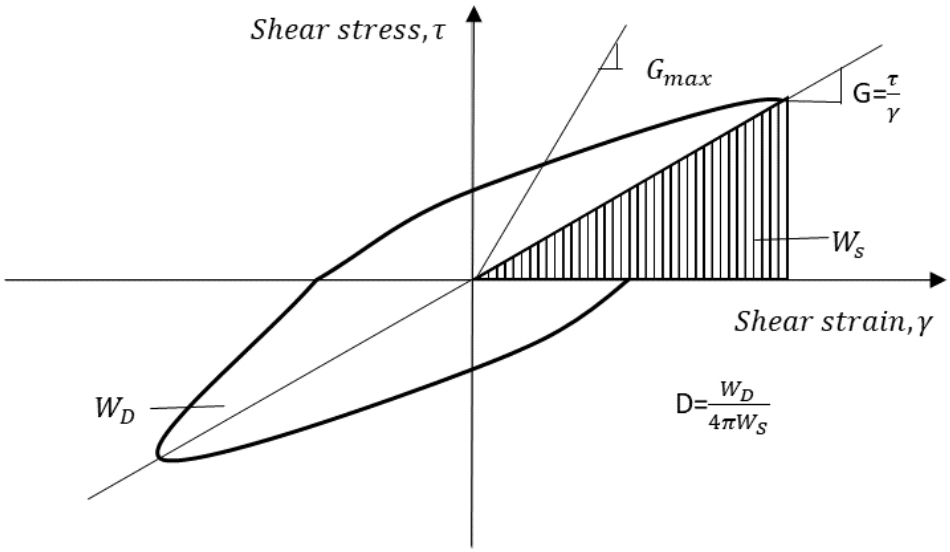

Figure 2.6. Hysteresis loop during a single loading cycle

As shown in Figure 2.6 and Equation (2.2), the Damping ratio (D) can be calculated using the formula, where W is the maximum strain energy, ΔW is the dissipated energy:

$$D = \frac{1}{4\pi} * \frac{\Delta W}{W} \qquad (2.2)$$

For the calculation of damping with correlations, the further equation expressed by (Tatsuoka, Iwasaki, & Takagi, 1978) and (Hardin & Drnevich, 1972) can be used:

$$D = f(\frac{G}{G_{max}}) \qquad (2.3)$$

However, it is more difficult to calculate the damping with the correlations because of its sensitivity and imprecise measurement compared to stiffness.

Figure 2.7 presents the damping ratio curves for clays and sands with the increasing plasticity index (PI) and OCR values. As can be seen, the damping ratio also increases with the increasing shear strain. However, with the increase of PI, the damping ratio values are lower.

The factors affecting the damping ratio are the same as those for the shear modulus. However, the number of loading cycles affects the damping ratio, while it has little effect on shear modulus. The impact of each factor on the dynamic soil properties is summarized by Seed and Idris (1970) and depicted in Table 2-1.

TABLE 2-1. Factors for testing soil's dynamic characteristics (Seed and Idris,1970)

Growing factor	**Shear modulus (G_{max})**	**Normalized shear modulus (G/G_{max})**	**Damping ratio (D)**
Confining pressure	Rises	Remains unchanged or rises	Remains unchanged or falls
Void ratio	Falls	Rises	Falls
Geological age	Rises	May rise	Falls
Overconsolidation ratio (OCR)	Rises	Unaffected	Unaffected
Plasticity index (PI)	Rises if OCR>1 When OCR=1, it is unchanged.	Rises	Falls
Cyclic strain	-	Falls	Rises
Cyclic loading frequency	Rises	Most likely unaffected if G and Gmax are obtained at the same interval	Remains unchanged or rises
Loading cycle number (N)	Reduces following N cycles of high cyclic strain but eventually increases	Drops during N major cyclic strain cycles (Gmax measured prior to N cycles).	Not important for the amount of loading cycles and moderate cyclic strain

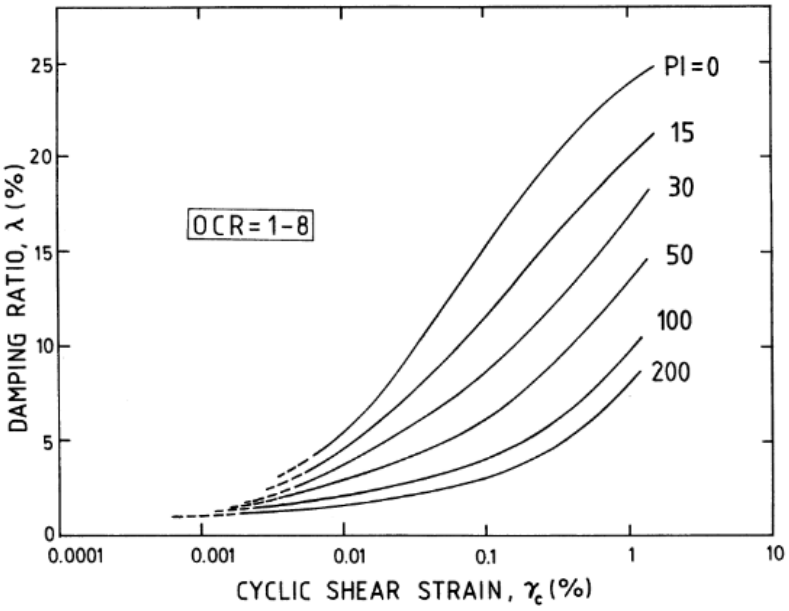

Figure 2.7. Damping ratio vs. shear strain for clays and sand (Vucetic & Dobry, 1991)

2.3.3. Normalized shear modulus reduction curve

Modulus reduction is defined as the proportion of G_{sec} to maximum shear modulus (G_{max}). A normalized modulus reduction curve is a depiction of cyclic shear strain. The normalized modulus reduction shown against the logarithm of the strain connection is a widely used graph.

The most commonly used formula to find the normalized shear modulus and the bounds is the hyperbolic law for the normalized deterioration curve (Equation (2.4)). It was initially put out by Hardin and Dvernich in 1972.

$$\frac{G}{G_{max}} = \frac{1}{1+\left|\frac{\gamma}{\gamma_{ref}}\right|} \qquad (2.4)$$

Where, γ_{ref} is a reference shear strain and

$$\gamma_{ref} = \frac{\tau_{max}}{G_{max}} \qquad (2.5)$$

Although the equation seemed obvious, the data didn't always reflect this real hyperbolic relationship. As a result, they modified the strain measurement by substituting "hyperbolic shear strain" for $\frac{\gamma}{\gamma_{ref}}$ on the horizontal plane. Thereafter, Darendeli (2001) proposed an updated hyperbolic model (Equation (2.6)):

$$\frac{G}{G_{max}} = \frac{1}{1+(\frac{\gamma}{\gamma_{ref}})^{a}} \qquad (2.6)$$

Where, a is the curvature coefficient. When the shear modulus ratio is equivalent to 0.5, the reference strain, as suggested, for example, by Stokoe et al., correlates to the shear strain magnitude. Here, γ_{ref} represents the shear strain amplitude at which 50% of the shear modulus is reduced.

Figure 2.8 depicts the often-employed and simple-to-use modulus degradation curves obtained by Vucetic and Dobry (1991). They proposed a graph for coarse-grained soils, although the figures were built on numerous cyclic loading studies for various soils, with the primary emphasis being on the effects of plasticity and over-consolidation (OCR) (Szilvágyi, 2018). In clays, the OCR significantly impacts the shear modulus, whereas in sand, it is vice versa, and there is little effect on the shear modulus. Moreover, it is noticeable that a reduced G/Gmax value with an increased number of cycles is caused by the reduction of inter-particle friction due to contact degradation.

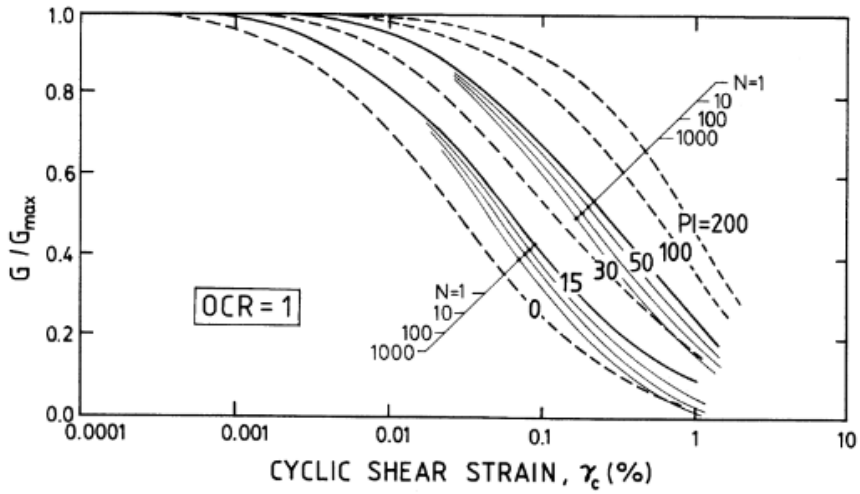

Figure 2.8. Cyclic stiffness degradation on sand and clay (PI=0) (Vucetic and Dobry, 1991)

Figure 2.9 shows the modulus degradation curve developed by Oztoprak & Bolton (2013), which is the best fit.

For that curve, they have analyzed an enormous amount of previously collected data and produced mean, upper-, and lower-bound curves by developing their fit using a modified hyperbolic formula:

$$\frac{G}{G_{max}} = \frac{1}{1+\left(\frac{\gamma-\gamma_e}{\gamma_{ref}}\right)^a} \qquad (2.7)$$

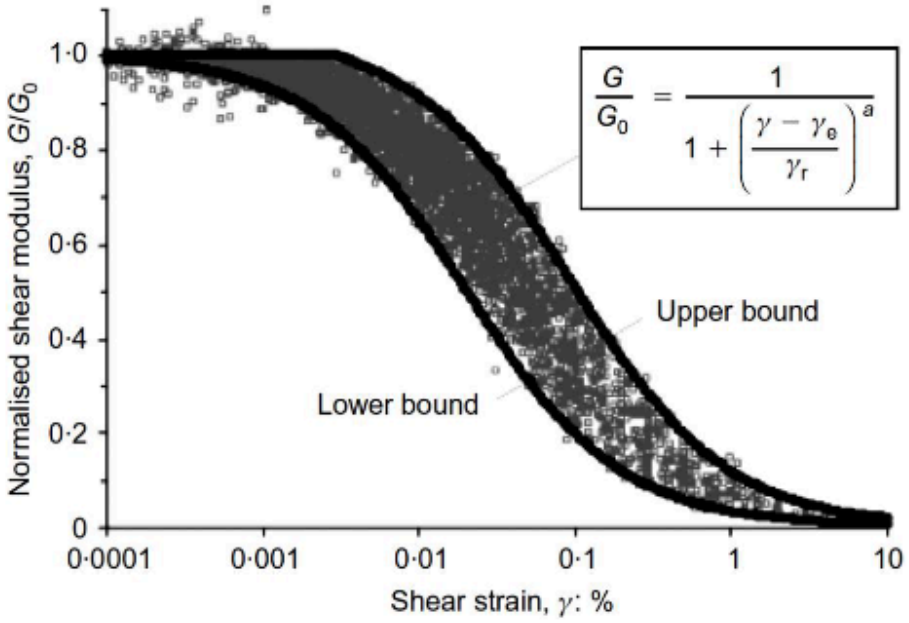

Figure 2.9 - a. Maximal fitting curves for modulus degradation (Oztoprak & Bolton, 2013)

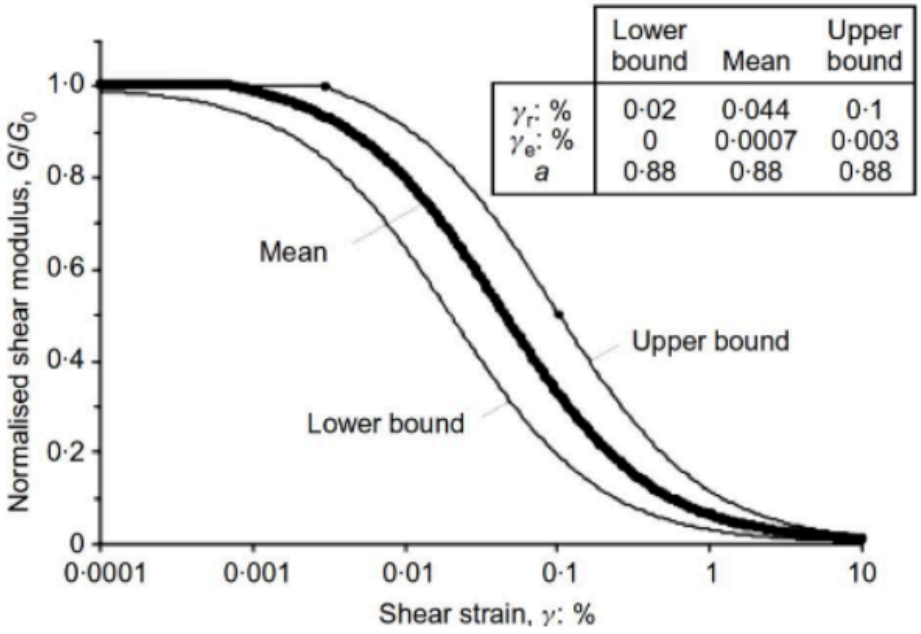

Figure 2.9 - b. Maximal fitting curves for modulus degradation (Oztoprak & Bolton, 2013)

TABLE 2-2. Constants of Equation (2.7) (Szilvágyi, 2018)

γ_e **(elastic threshold strain), %**	γ_{ref} **, %**	**a**	**Bound type**
0	0.02	0.88	lower
0.0007	0.044	0.88	mean
0.003	0.1	0.88	upper

2.4. Application of dynamic soil characteristics

Understanding site response analysis, the dynamic behavior of retaining walls and foundations, and soil-structure interaction all depend on dynamic soil features. These characteristics are crucial when evaluating how earth buildings, like rockfills and dams, will react to earthquakes and planning them for seismic resistance. Assessing dynamic soil characteristics becomes even more important in areas where dynamic loading is a major problem. The precise identification of dynamic soil parameters is crucial to solving the many problems caused by dynamic loading in soil dynamics and geotechnical earthquake engineering.

Dynamic soil properties are used to analyze ground vibrations and earthquake-induced wave propagation, solve soil liquefaction issues, and assess the dynamic pressure, distortion, and strength attributes of soils. These characteristics are also essential for evaluating how marine debris and its supported structures react to ocean waves, establishing a flexible load capacity for shallow base concepts, and guaranteeing the structural integrity of embankments and dams in seismic circumstances (Hoque, 2016). They are also used in the design of pavements undergoing traffic-induced stresses, embed bases and piles impacted by dynamic loads, and foundations for vibrating machinery. Furthermore, dynamic soil parameters are essential when evaluating the effects of blasting in mining and construction operations.

Chapter 3. Methodology

3.1. Methods to determine dynamic soil properties

In soil dynamics and geotechnical earthquake engineering, dynamic properties are crucial to resolving several problems. These properties are investigated using various experiments in both laboratory and real-world environments.

3.1.1. Field tests

In situ tests classify according to strain levels and surface testing standards. Seismic geophysical investigations create transient or steady-state stress waves to replicate how soil reacts to dynamic stressors such as earthquakes or machine vibrations (Szilvágyi, 2018). These tests primarily calculate the small strain stiffness (G_{max}) and shear wave velocity while considering the geological conditions, depth, site size, and structural significance. Field tests are essential for comprehending soil parameters because of their in-situ measurements. Among its benefits are the absence of the necessity for sampling, the ability to assess sizable amounts of soil, and the induction of deformations akin to the issue at hand. Moreover, many tests can be done in situ, such as SPT, CPT, and seismic refraction (Abdialim et al., 2024), as indicated in Table 3-1.

They are not without restrictions since the particular feature of interest in the soil can often not be measured directly; instead, it must be ascertained via theoretical analysis or empirical correlation. Field examinations usually measure the top 30 meters of soil to ensure that code specifications—like those for Eurocode 8 soil classes—are satisfied. Notwithstanding its shortcomings, the useful knowledge gathered from field experiments greatly advances our comprehension of soil dynamics in actual situations.

3.1.2. Laboratory tests

Laboratory experiments are essential for the in-depth analysis of dynamic soil parameters because they offer important insights into how soils behave under various loading scenarios. These experiments, which utilize tiny specimens that are thought to be typical of larger soil

bodies, are crucial for comprehending how soils react to dynamic pressures (Szilvágyi, 2018). Laboratory testing is difficult because of the inherent changes in soil composition, particularly when using reconstituted samples. Reconstruction may change the soil's natural composition and properties, affecting the reliability of the test findings. Anisotropic circumstances in both real and recreated specimens can also impact the accuracy of the results. The factors essential for comprehending how soils react to dynamic stressors are the subject of laboratory testing for dynamic soil attributes. During these tests, shear wave velocity and small strain stiffness (G_{max}) are frequently assessed. The ability of the soil to transmit seismic waves and withstand dynamic loading is evaluated by these characteristics, which are crucial for earthquake engineering and geotechnical design.

Regarding the difficulties in conducting laboratory experiments, the results substantially impact a range of geotechnical uses. The data gathered from these experiments is used to evaluate the interaction between soil and structure, create seismic design standards, and create practical plans for reducing the influence of dynamic stresses on structures. Because of it, for that thesis work, the dynamic soil properties are conducted by laboratory test. As there is a lack of data on the dynamic properties of well-graded sand with silt in Kazakhstan for low-to-intermediate strain, the resonant column (RC) and cyclic torsional shear (CTS) tests will be used (Table 3-1).

TABLE 3-1. Measurement methods of dynamic properties (Kumar et al.,2013)

In-situ tests		**Laboratory tests**	
Low strain (<0.001%)	High strain (>0.01%)	Low strain (<0.001%)	High strain (>0.01%)
Seismic reflection	Standard penetration test (SPT)	Resonant column test	Cyclic triaxial
Seismic refraction	Cone penetration test (CPT)	Ultrasonic pulse test	Cyclic direct shear
Steady-state vibration	Dilatometer test (DMT)		

In-situ tests		Laboratory tests	
Low strain (<0.001%)	High strain (>0.01%)	Low strain (<0.001%)	High strain (>0.01%)
Spectral analysis of surface waves (SASW)	Pressumeter test (PMT)	Bender element	Cyclic torsional shear
Multi-channel analysis of surface waves (MASW)			
Seismic borehole tests			
Seismic cone surveys			

3.2. Device - Resonant Column Apparatus

The resonant column apparatus (RCA) is more advantageous for determining dynamic soil parameters, as it can conduct both resonant and cyclic torsional shear tests. The RCA is used to study the dynamic properties of geomaterials at low strain levels (Sakshi & Sebastian, 2023). It involves applying a small cyclic torsional force to a prepared soil specimen using an electromagnetic instrument. After measuring the sample's reaction with an accelerometer and adjusting the load's frequency to reach the resonance frequency, the shear modulus (G) is computed using the specimen's geometry and device characteristics (Szilvágyi, 2018). In some variants, the use of a hollow cylinder reduces strain variations. This method works well for examining the effects of small strain levels (between 10^{-6} and 10^{-2} percent), confinement pressure, and time. The stimulation of torsional vibration will be carried out throughout a voltage amplitude ranging from 0.005 V to 1 V. The Resonant Column apparatus of the GDS instruments was used in this investigation, which is depicted in Figure 3.1.

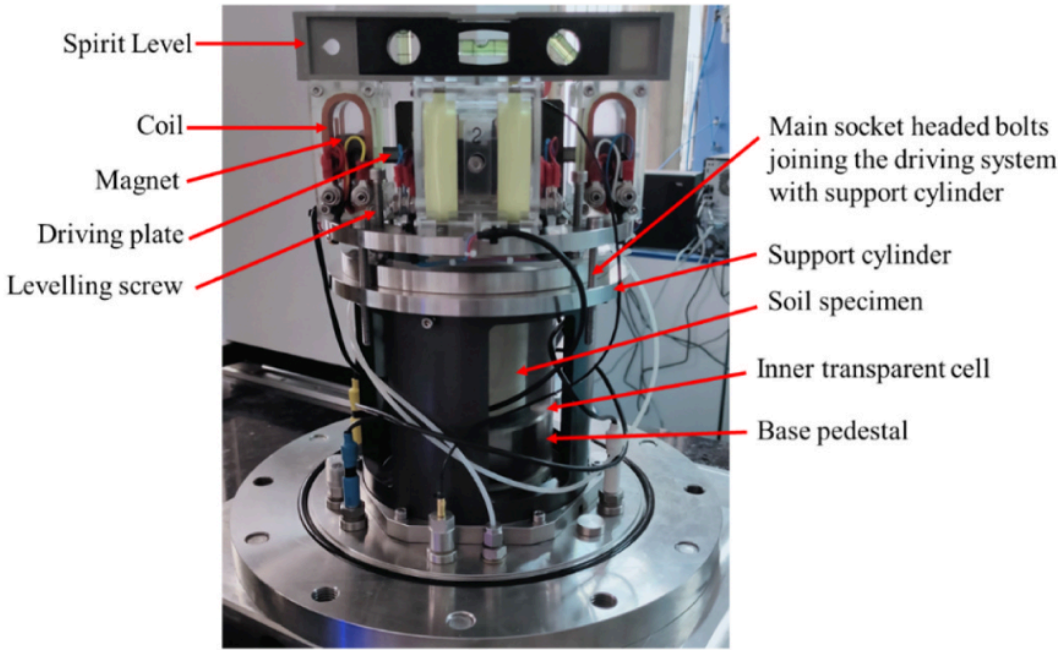

Figure 3.1. RCA with its elements (Sakshi & Sebastian 2023)

The resonant frequency, along with the features of the apparatus and specimen, is used to calculate the shear wave velocity (V_s), associated shear modulus (G), and shear strain amplitude (γ). The current study aims to improve our understanding of how confining pressure affects the dynamic characteristics of the well-graded sand with silt in Astana. In drained circumstances, confining pressures vary from 50 kPa to 200 kPa in increments of 50 kPa.

There are several benefits to the GDS RCA system. It has an extremely strong bond connecting the coils and the support plate, among other things. In order to do this, each pair of coils is enclosed in a Perspex jacket and firmly attached to the base plate. To connect all the coils together, a circular plate that is magnetically neutral is attached to the top of each Perspex block. The support cylinder's unique design offers this component its greatest rigidity. Moreover, the equipment was intended to reduce the dampening impact. In free vibration decay, which occurs when the power is cut off at resonance, the motion of the magnets in the coils often produces the back electromagnetic field. This leads to significant equipment damping errors (GDS, 2010).

3.3. Sample preparation

Several suggested sample preparation approaches have been suggested, such as air-pluviation, wet-tamping, moist-vibration, spooning, and raining techniques (Ishihara et al.,1978). It is acknowledged that there are variables affecting soil strength, including sample preparation techniques and testing protocols (Silver et al.,1980).

Researchers discovered that specimen diameter (d) changes might significantly affect cyclic strength; samples with a d= 300 mm were around 10% lower than specimens with a d= 70 mm (Wong et al., 1975). This was the reason for choosing the sample diameter size of 70mm and height of 140 mm.

All the samples collected try to maintain the original soil structure and composition, which are considered ideal for testing. A crucial stage in geotechnical study is sample preparation for soil samples obtained from construction sites in Astana. The soil samples are defined as well-graded sand with silt. To guarantee that the results of any further tests are accurate, these samples were prepared by maintaining the optimum moisture content of 14.0% and maximum dry density. Proper labeling, classification, and storage in a controlled environment are crucial to avoid modifications or contamination.

The sample preparation and testing procedures were carried out in compliance with ASTM D4015 2014 guidelines. It takes careful work to shape samples into uniform sizes for different scientific testing. The initial density and moisture content must be preserved throughout this process to correctly represent field conditions. This thorough sample preparation process contributes to a thorough understanding of soil behavior under various loading situations by improving the accuracy of ensuring dynamic soil property testing.

Chapter 4. Testing procedure

Following the processing of the soil sample, the resonant column test setup is installed by next steps (Figure 4.1):

1. Six screws are used to fasten the internal support cylinder to the bottom plate firmly.
2. To aid with saturation, drainage lines are attached to the soil's upper cover.
3. After carefully positioning the electromagnetic drive mechanism on the sample and leveling it with a spirit level, four screws are used to secure it to its upper cap.
4. Because the drive mechanism is centralized, the magnets in the coil stay aligned for unrestricted movement.
5. The accelerometer wire is connected to the electromagnetic drive system, which is securely fastened to the support cylinder using screws.
6. The setup is finished by lowering the confining pressure tank and fastening it to the bottom surface with six screws (Dutta, 2015).

Software packages GDSLab and GDSRCA will be utilized to process the data. Before starting the RC and CTS tests, the sample should be saturated and consolidated using the steps described below:

1. Flush the equipment and fill it with de-aired water for the pore pressure system. Make sure that there is no air voids in the equipment by checking for the bubbles;
2. Attach the filter papers to both (top and bottom) sides of the sample to fasten the consolidation stage and spread the water from the pore pressure system;
3. Equip the sample with two latex membranes to decrease the air diffusion;
4. Install the sample to the cell;
5. Saturate the sample by back pressure method;
6. Gradually impose a small amount of cell and back pressure, so the air in the intergranular gaps was dissolved;
7. Gradually rise the pressure till the Skempton’s B-value was more than 0.95 to guarantee that the test sample was properly saturated;
8. Open the drainage valves that connected the specimen to the volume change device and start the consolidation (Sas et al.,2017);

9. Use the back pressure that was applied in the previous saturation phase, but vary the cell pressure according to the mean effective stress;
10. Measure the axial deformation and volume change of the sample;
11. Update the void ratio at every loading step;
12. The consolidation process persisted until the first phase of consolidation concluded, which was typically approximately one day (sometimes even 48 hours) (Fernández-Guzmán et al.,2014);
13. Start the data extraction procedure (RC and CTS tests).

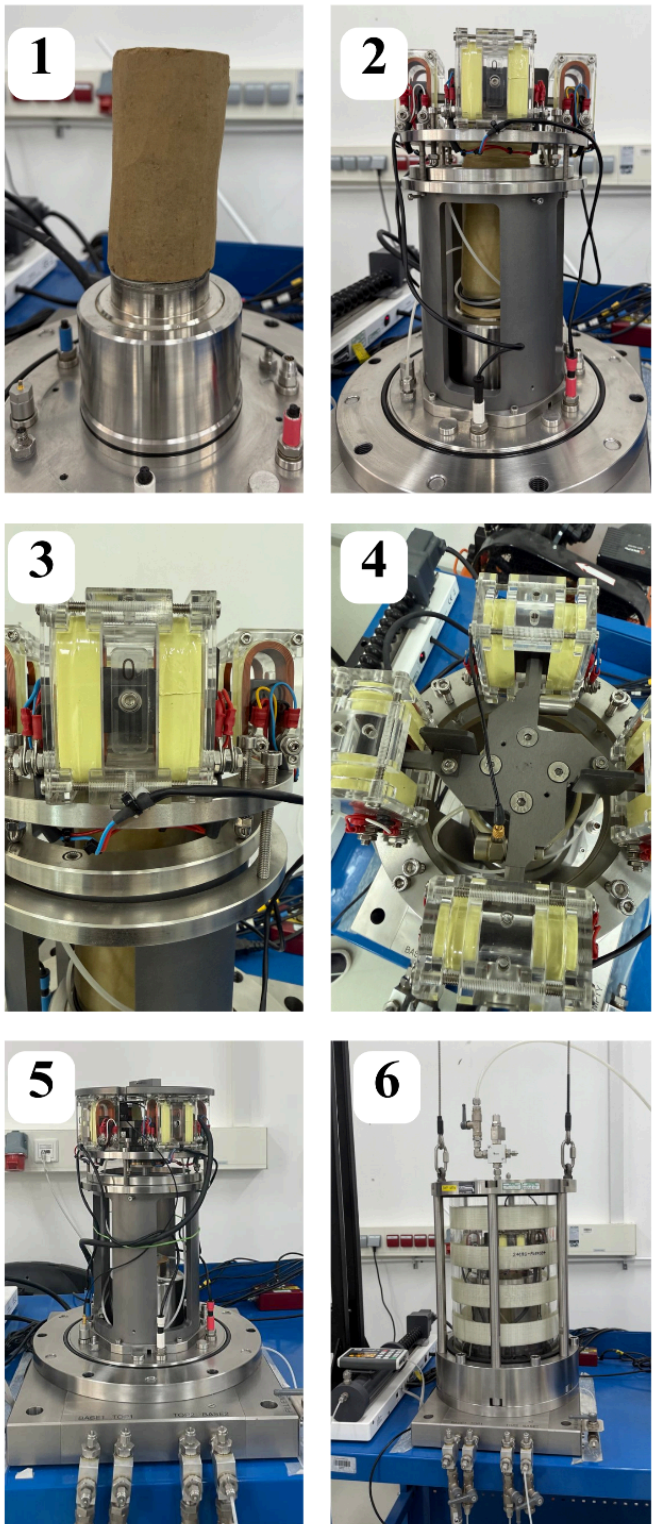

Figure 4.1. Configuring a test to run RCA tests

The soil sample is initially saturated and subsequently consolidated with the aid of GDSLab software. While the consolidation phase contributes to learning how soils respond to applied loads, including long-term settlement behavior, the saturation phase ensures that soil samples are in a genuine, fully saturated state, imitating field circumstances (B-value>0.95). These stages are crucial for precise geotechnical analysis, foundation design, and soil and rock material behavior prediction in various engineering and construction projects.

4.1. Resonant Column Test

There are several types of resonant column apparatus; the most popular are free-free, fixed-free, and fixed-fixed. The fixed-free solution is the most suitable for determining dynamic soil properties, and it will be used in our test. Using an electromagnetic drive system, a sinusoidal torque is applied to the object to conduct the RC test. The driving system comprises a backing cylinder with four sets of wire coils and a four-arm rotor with a strong magnet attached to each arm. The drive plate (shown in Figure 4.2) is connected to the object during the sample preparation, and the base cylinder's height is changed to enable the magnets to be placed in the center of the wire coils. A sinusoidal voltage is provided to the coils to impart the torque on the specimen. The resulting magnetic field causes the driving plate to oscillate as an outcome. The resonance frequency is easily found by graphing the accelerometer's peak output values versus the applied voltage frequency.

Four electromagnets were employed in two distinct directions to complete the test for the torsional and flexural modes (Dutta, 2015). The magnet configuration for the torsional and flexural tests is shown in Figure 4.3. The two magnets operate in series throughout the torsional mode, applying a net torque on the soil specimen. A single set of magnetic coils generates an additional horizontal force at the top of the sample to apply the flexural stimulation. At first, a low-frequency setting is used. The frequency is then progressively raised after that. The sample's resonant frequency may be found where the amplitude peaks.

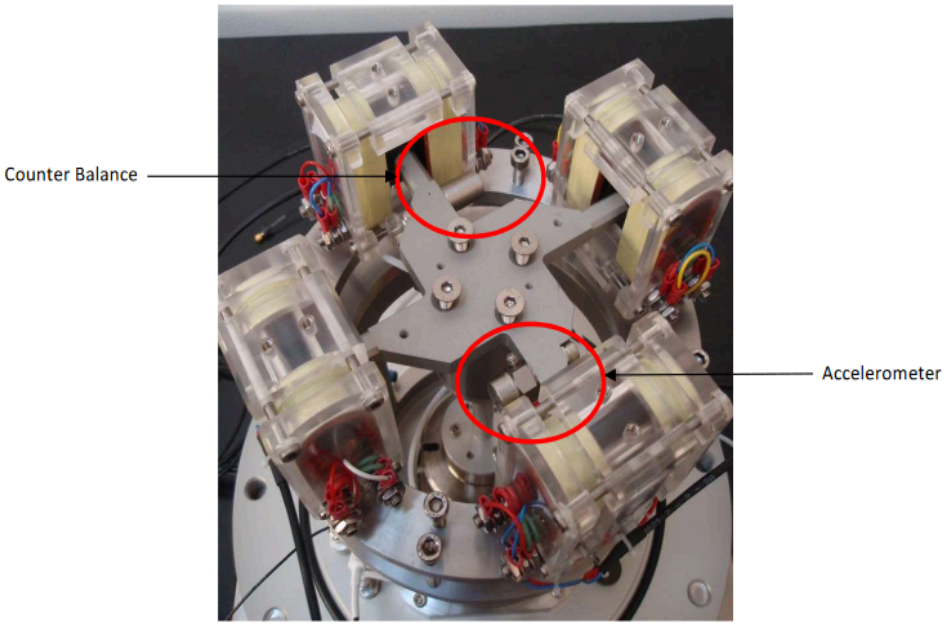

Figure 4.2. Electromagnetic system of RCA (GDS Resonant Column, 2010)

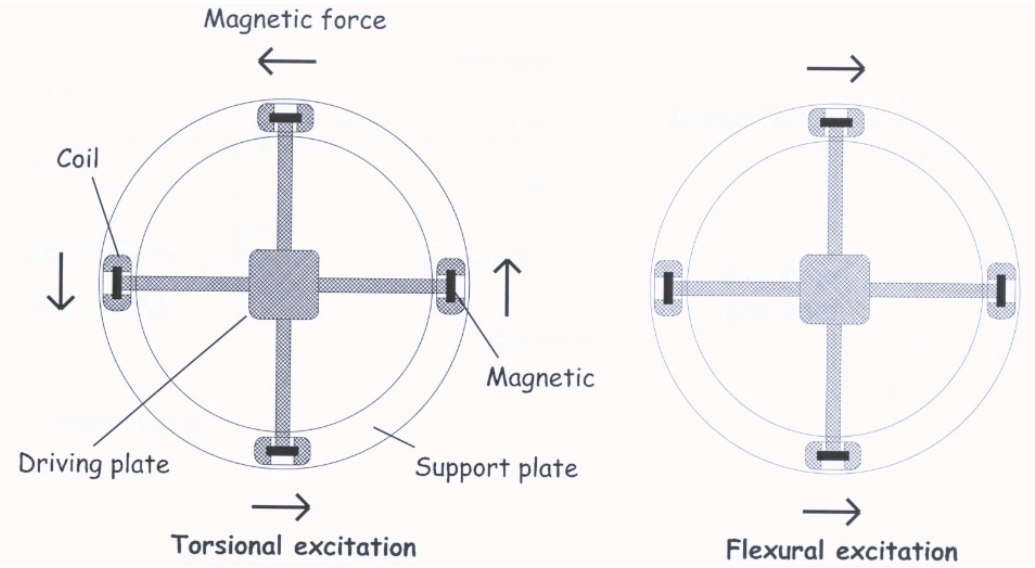

Figure 4.3. Torsional and flexural excitation (GDS Resonant Column, 2010)

The configuration of the resonant column device is shown in Figures 4.4 and 4.5. The resonant column controller receives a command from the computer to produce a sine wave signal with the required amplitude when the RC test is initiated. After being amplified by the power amplifier, the signal is transmitted to the resonant column controller. The signal is subsequently divided into four equal portions and delivered to the four coils of RCA. The torque produced by

the electromagnetic driving mechanism causes the specimen to shake. The charging signal that the accelerometer captured during the vibration passes to the charge amplifier, which then forwards it to the computer via a resonant column controller. The amplitude versus frequency is shown on the computer.

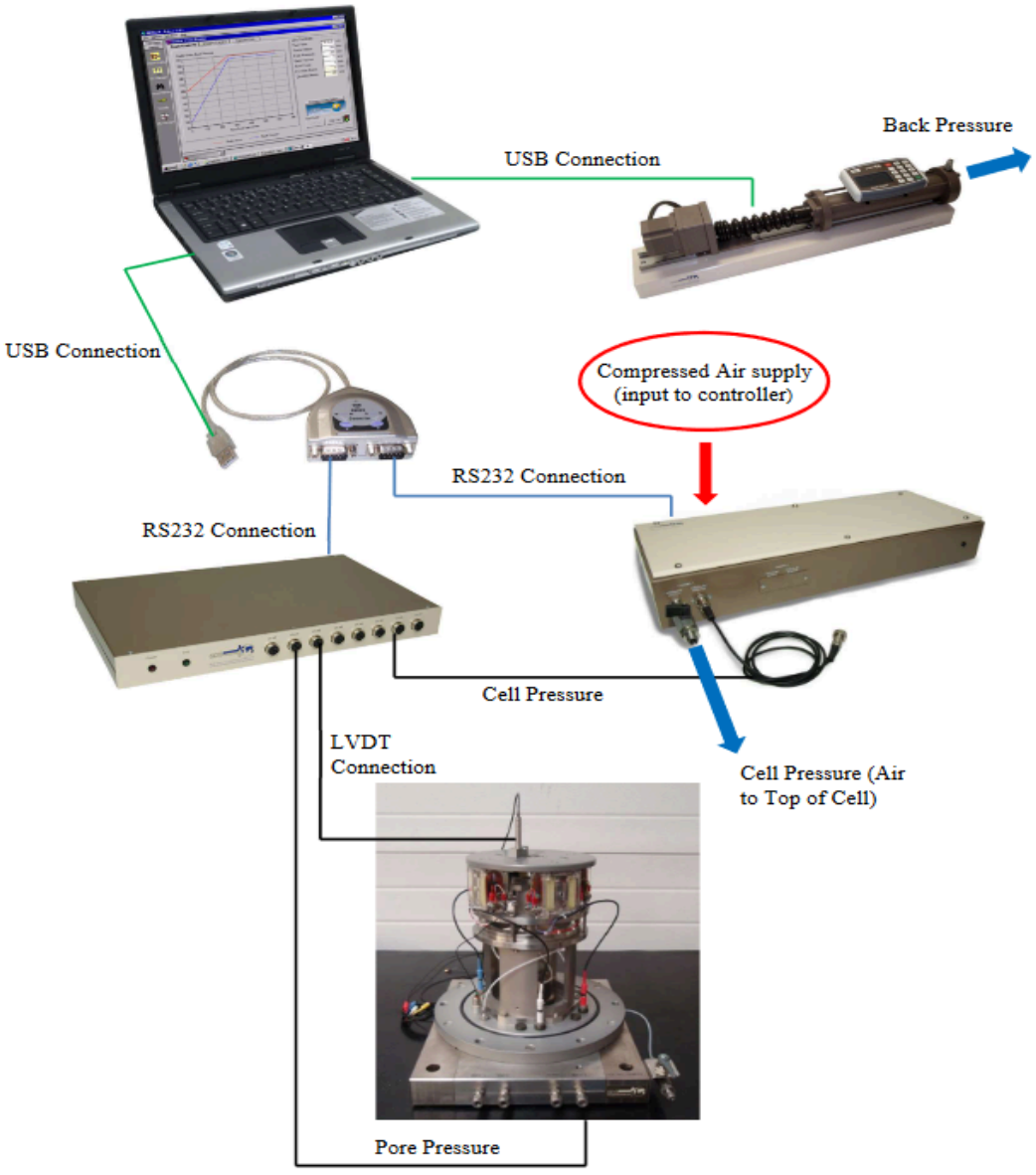

Figure 4.4. Schematic diagram of RCA system (GDS Resonant Column, 2010)

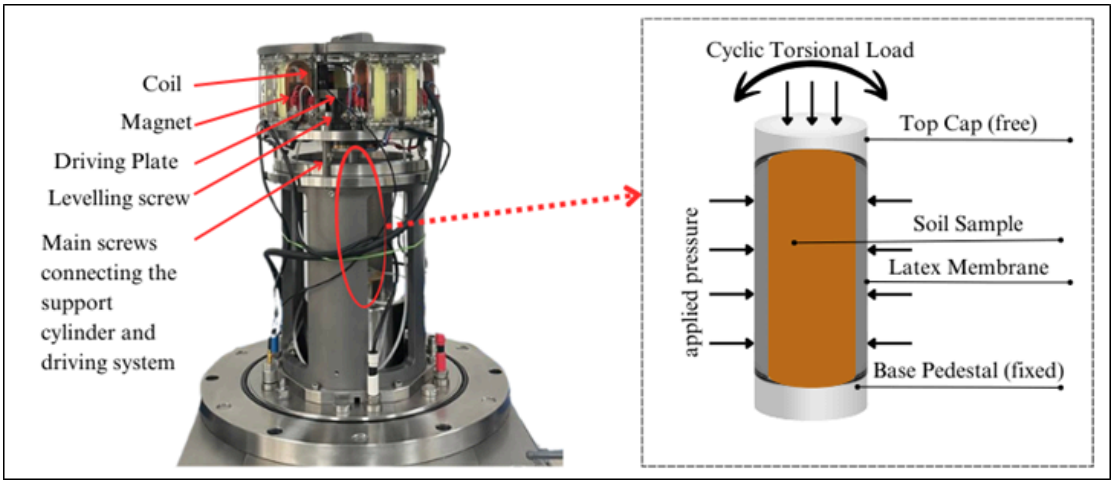

Figure 4.5. Schematic diagram of RCA system

4.1.1. Shear modulus establishment

To determine the shear modulus (G) from the resonant column test, the shear wave velocity should be calculated first. It can be derived from the formula given below:

$$v_s = \frac{2\pi f L}{\beta} \tag{4.1}$$

Where f - frequency, L - length, β is derived from the Equation (4.2):

$$\frac{I}{I_0} = \beta * tan(\beta) \tag{4.2}$$

I_0- mass polar moment of inertia of the equipment. As a result, data from the resonant column test needs to be decreased. Since the drive system's shape makes it impossible to calculate analytically, its value is determined empirically by calibration, which is covered in the following section.

I - mass polar moment of inertia of the sample, which is calculated by:

$$I = \frac{md^2}{8} \tag{4.3}$$

Finally, using all of these values, the shear modulus can be calculated by the following equation:

$$G = \rho * v_s^2 \tag{4.4}$$

Where ρ = bulk density.

4.1.2. Damping ratio establishment

After determining the resonance frequency, the stimulation power was turned off, allowing the specimen to vibrate at will. The GDSRCA software for Resonant Column test calculates the viscous damping ratio (D) based on the free vibration decay curve's form (GDS Resonant Column, 2010). The accelerometer installed on the RC drive plate determines that curve. To quantify the free vibrations that come from applying a sinusoidal wave to the sample, the excitation is then turned off, as seen in Figure 4.6. One may determine the decay curve by calculating the log of the ratio of the amplitudes of succeeding cycles.

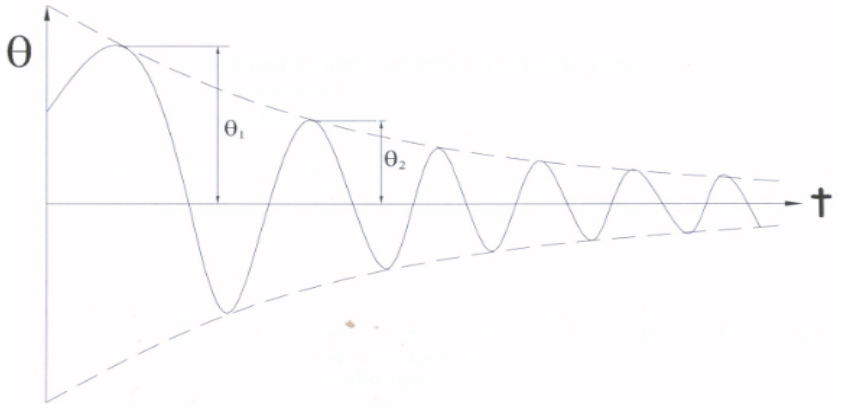

Figure 4.6. Free vibration decay curve (GDS Resonant Column, 2010)

Plotting the logarithmic decrement against the period number yields the logarithmic peak amplitude. This plot should, in principle, follow a straight line. This line's best-fit slope equals the logarithmic decrease. In actuality, the computation often involves ten to fifty cycles. Your selected "No. of Cycles" will be the basis for the program's calculation of a line of best fit. Damping ratio (D) is calculated based on these equations:

$$D = \sqrt{\frac{\delta^2}{4\pi^2+\delta^2}} \qquad (4.5)$$

Or

$$D = \frac{1}{2\pi n} ln(\frac{Z_0}{Z_n}) \qquad (4.6)$$

Where, δ - logarithmic decrement, Z_0- vibration amplitude following the turn-off of the excitation power, Z_n- vibration amplitude after the nth cycle, n - number of cycles.

4.2. Cyclic Torsional Shear Test (CTS)

The CTS test is followed by the resonant column test. Here, the sine-wave cyclic torsional vibration with a low frequency (0.1–10 Hz) and a predetermined amplitude is applied along the test sample's vertical axis for a particular amount of cycles (Sakshi and Resmi, 2023). To measure the angle of twist (α), proximitors were positioned below the test specimen. Equation (4.7) gives the combination of the strain calibration factor (C_s) and the applied output voltage to yield α owing to the imposed torque.

$$\alpha = C_s * V_t \quad (4.7)$$

Equation (4.8) gives the torque (T) that results from applying torsional vibration to the drive system, which is derived from the initial voltage delivered to the system.

$$T = C_t * V_t \quad (4.8)$$

The following formula can be used to express the specimen's shearing stress magnitude, where R-radius, J-polar moment of inertia:

$$\tau = R * T/J \quad (4.9)$$

The specimen's torque and twist characteristics produce a plot that resembles a hysteresis loop, and the G_{sec} is obtained from the gradient of the line connecting the loop's two endpoints (Sakshi and Resmi, 2023). The sample was first excited at the lowest possible voltage to conduct the CTS tests, equivalent to an estimated strain amplitude of 10^{-2} %. For additional testing, the voltage is gradually raised after the first excitation throughout a spectrum of strain values, ultimately reaching an estimated strain amplitude of 1%.

4.3 Calibration

A test is run on a calibration bar to empirically determine its resonant frequency in torsion and flexure to calculate I_0 and I_y. It is accomplished by using metal calibration bars (shown in Figure 4.7), which have mechanical characteristics that have been established, in place of the specimen to calibrate the device. A variety of calibration weights are put into the drive system, and the test is performed on three occasions for each calibration bar (a total of three bars). After each test, the new resonant frequency is determined.

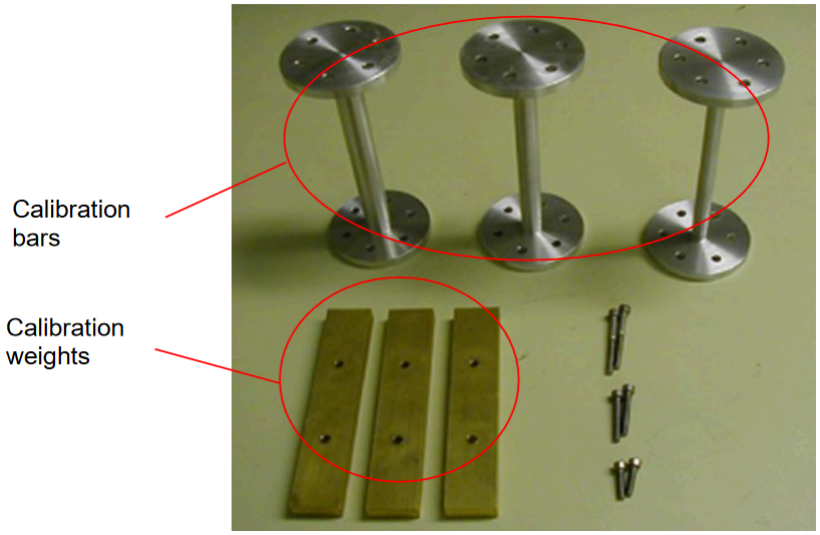

Figure 4.7. Calibration bars and weights

All of the tested resonant frequency results are written to the Excel spreadsheet (Figure 4.8) provided by GDS company, where the mass polar moment of inertia of the added mass is then plotted against $1/\omega^2$(Figure 4.9). The value I_0 serves as the intercept on the I_{am} axis, while k serves as the gradient to construct a straight line.

As shown in the Figure below, when the bar's diameter increases, the resonance frequency also rises.

Resonant Column Testing- calibration of drive system

Element	Mass polar moment of inertia I of system kg m²	Total Mass polar moment of inertia I kg cm²	Resonant frequency of calibration bar Hz	angular velocity at resonance ω rads/s	ω²	1/ω²	Intercept (Iam)
Aluminium Bars							
15mm Bar							
top plate	8.2774E-06	8.28E-06	73.5	461.8141	213272.3	4.68884E-06	
weight #1	0.0001144	0.000123	72.1	453.0177	205225	4.8727E-06	
weight #2	0.0001144	0.000237	71.2	447.3628	200133.5	4.99667E-06	
weight #3	0.0001144	0.000351	70.6	443.5929	196774.6	5.08196E-06	-0.0040091
12.5mm Bar							
top plate	8.2774E-06	8.28E-06	52.2	327.9823	107572.4	9.29607E-06	
weight #1	0.0001144	0.000123	51.5	323.584	104706.6	9.55049E-06	
weight #2	0.0001144	0.000237	50.2	315.4159	99487.19	1.00515E-05	
weight #3	0.0001144	0.000351	50.1	314.7876	99091.22	1.00917E-05	-0.0033705
10mm Bar							
top plate	8.2774E-06	8.28E-06	33.8	212.3717	45101.72	2.21721E-05	
weight #1	0.0001144	0.000123	33.3	209.2301	43777.22	2.28429E-05	
weight #2	0.0001144	0.000237	32.8	206.0885	42472.46	2.35447E-05	
weight #3	0.0001144	0.000351	32.4	203.5752	41442.86	2.41296E-05	-0.0038469
						Average Iam	-0.0037422

Added Masses

Calibration Weights

Width	0.02	m
Length	0.1	m
Mass	0.132	kg
Iam	**0.000114**	

Calibration bar

(added mass is simply the top disk)

Diameter	0.05	m
Height	0.005	m
Volume	9.82E-06	m2
Density	2698	kg/m2
Mass	0.026488	kg
Iam	**8.28E-06**	**md2/8**

Figure 4.8. Excel spreadsheet for the calibration calculation

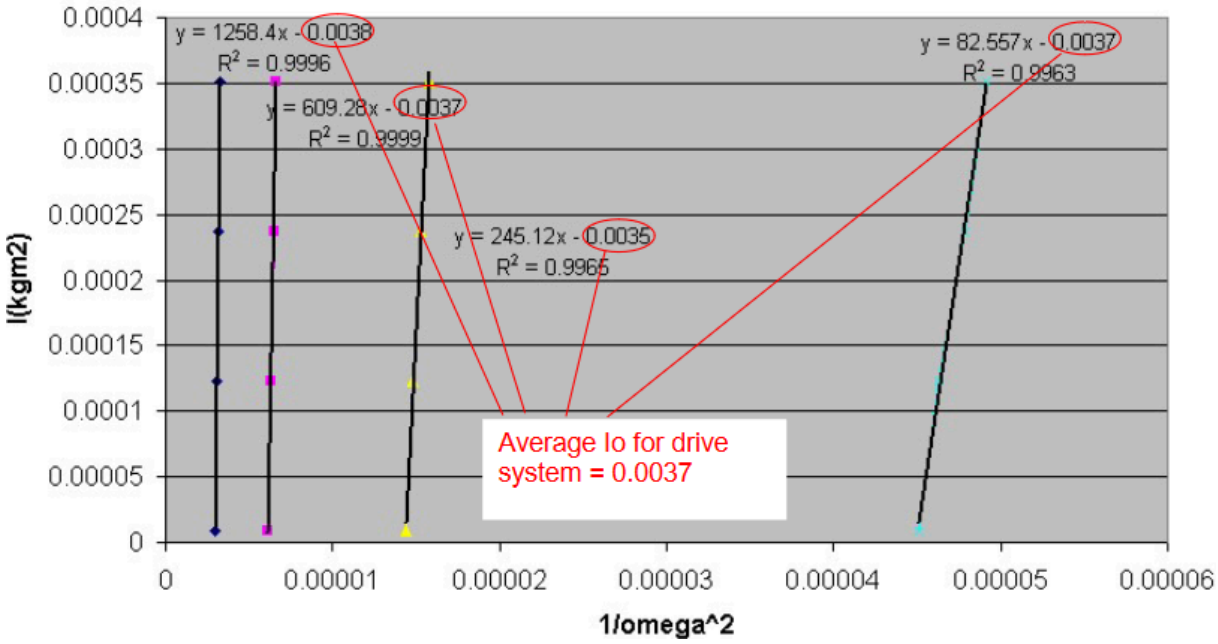

Figure 4.9. Example of the calibration (I_{am} vs. $1/\omega^2$)

Chapter 5. Physical Properties of the Soil

As seen in Figure 5.1, the soil samples will be taken at a location in Astana, Kazakhstan. The source of the material is a nearby building site. The near-surface layer was determined by routine compaction tests to be well-graded sand with silt, as shown in Figures 5.2 and 5.3. It had a maximum dry density (MDD) of 1.868 kN/m³ and an optimum moisture content (OMC) of 14.0%. This soil is categorized as well-graded sand with silt (SW-SM) by the Unified Soil Classification System (ASTM D2487). Important physical characteristics that are necessary for additional computations are included in Table 5-1, including dry bulk density, liquid limit (LL), plastic limit (PL), and plasticity index (PI). These metrics show comparatively low plasticity, which is typical of fine-particle, sandy soils. The ASTM D4318 guidelines were followed in determining the LL, PL, and PI values. Several tests were carried out to guarantee accuracy because of the low fine content.

Scanning electron microscopy (SEM) high-resolution pictures of the sand particles demonstrated their sub-angular form (Figure 5.4). Sand with this shape is commonly found in places with little transportation, such building sites or newly exposed deposits. According to earlier research, particle form has a major impact on soil collapse and settlement behavior under shear and wetness circumstances (Mahinroosta and Oshtaghi, 2021). The features of the silt-containing well-graded sand are further explained in Figure 5.4 and Table 5-1.

Both main and minor elements are present in the material's complex mineralogical structure, as shown by its chemical makeup. The high quartz concentration characteristic of sandy soils is highlighted by the main ingredients, including silicon dioxide (SiO_2) at 42.06%, iron oxide (FeO_3) at 21.16%, and aluminum oxide (AlO_3) at 12.35%. AlO_3 and FeO_3 indicate the presence of clay minerals and iron compounds, which improve soil cohesiveness. Sulfur trioxide (SO_3), potassium oxide (K_2O), magnesium oxide (MgO), calcium oxide (CaO), and titanium dioxide (TiO_2) are minor constituents. These components, while in lesser amounts, may have an impact on the soil's chemical behavior and durability in different environmental settings.

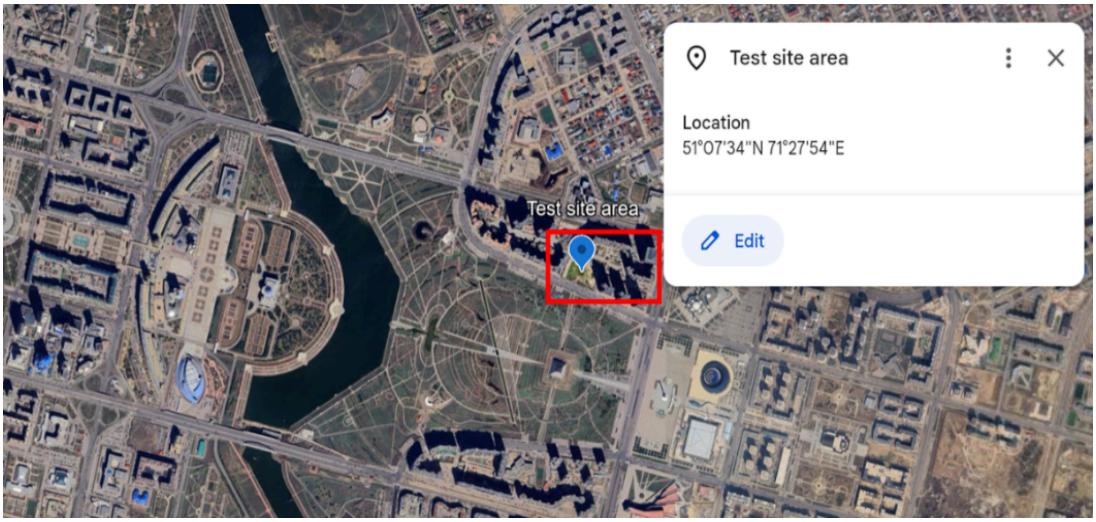

Figure 5.1. Testing site in Astana, Kazakhstan

Figure 5.2. Well-graded sand with silt in Astana, Kazakhstan (Sagidullina et al., 2025)

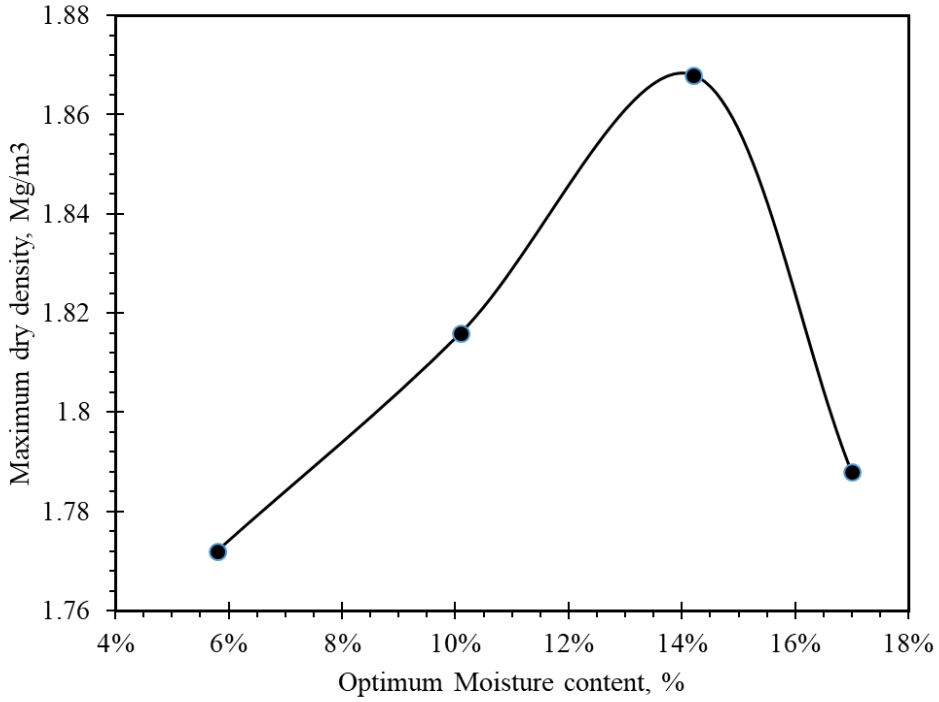

Figure 5.3. OMC and MDD of well-graded sand with silt

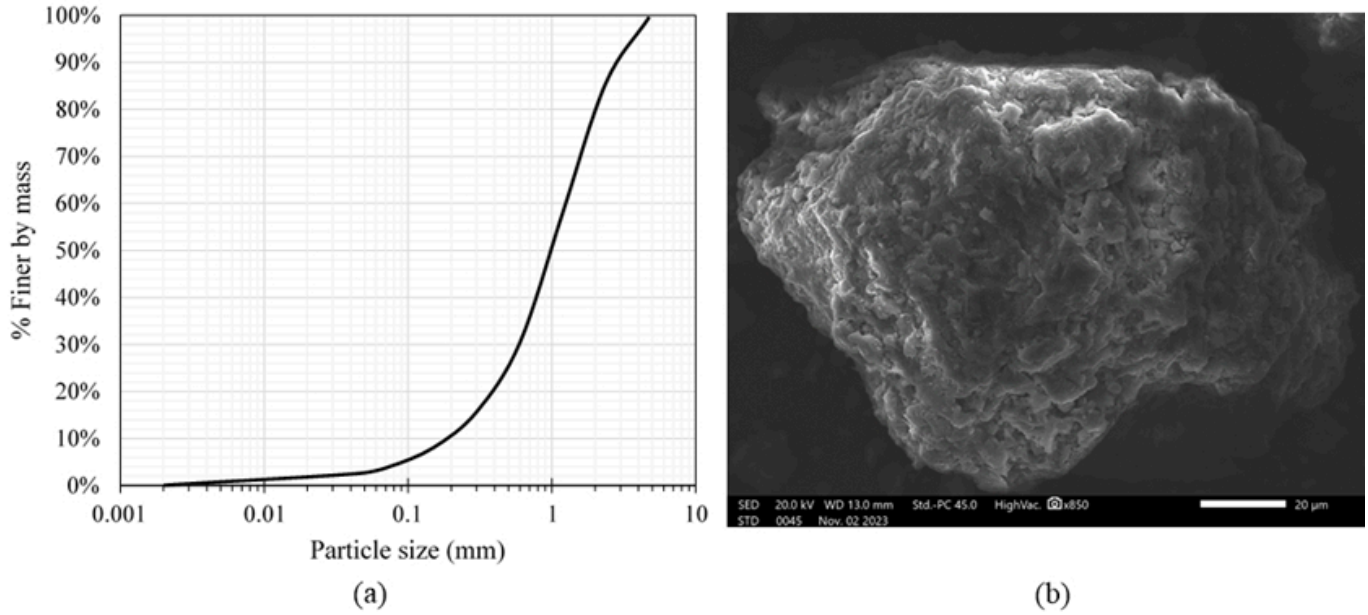

Figure 5.4. (a) Particle size distribution curve; (b) SEM image of the well-graded sand with silt

TABLE 5-1. Physical characteristics of the soil specimens

PROPERTIES	VALUE
USCS classification	SW-SM
Liquid Limit (LL)	32
Plastic Limit (PL)	22
Plasticity Index (PI)	10
Dry Bulk density (ρ, Mg/m^3)	1.4
D10 (mm)	0.3
D30 (mm)	0.95
D60 (mm)	2
Uniformity coefficient, C_u	6.7
Coefficient of curvature C_c	1.5

Chapter 6. Test Results

6.1. Calibration results

Figure 6.1 shows calibration results obtained using the method in Chapter 4 and with conformity with ASTM D4015 (2015). Each aluminum bar had three runs in the test using different calibration weights connected to the driving system. The resonance frequency and associated peak amplitude were recorded at a predetermined input voltage for every trial (Shinde and Kumar, 2021). Aluminum specimens were found to have resonance frequencies between 32.4 Hz and 73.5 Hz (Figure 6.1). From that Figure, we can derive the average I_0, which equals -0.00374.

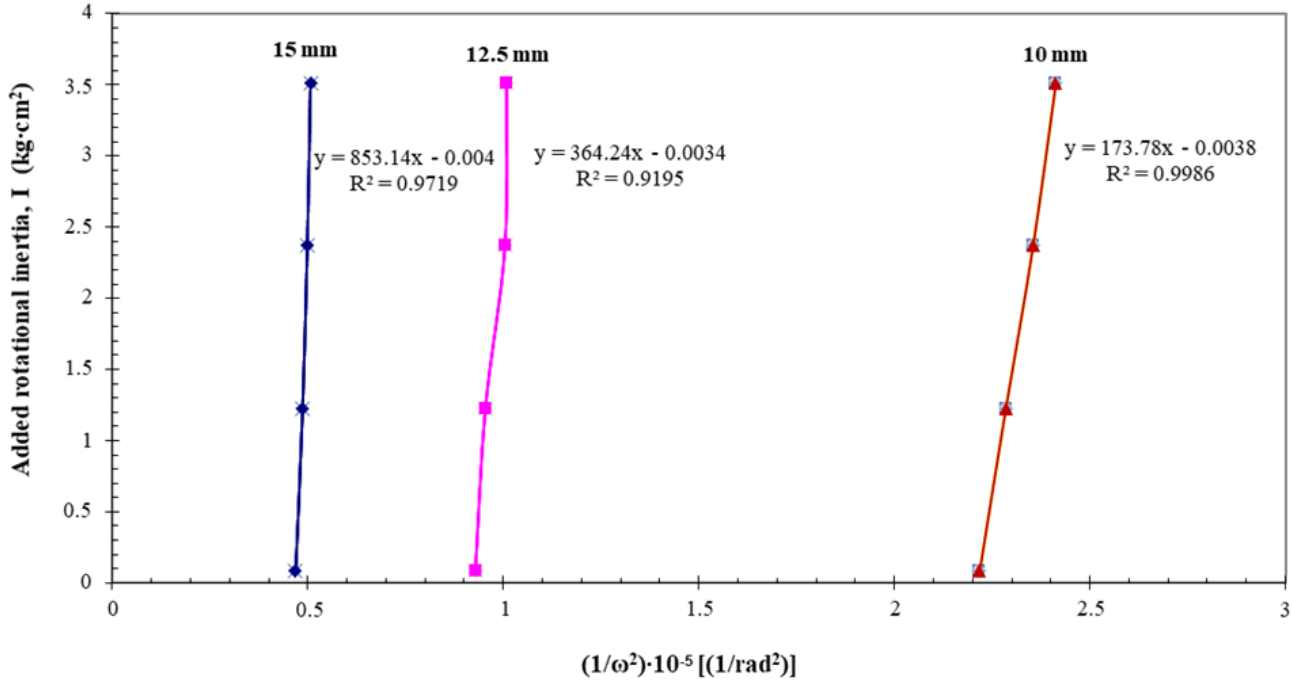

Figure 6.1. Calibration results for aluminum bars with varying diameters using added masses

It is necessary to determine I_0 precisely in order to figure out the soil specimens' shear modulus (G). I_0 It is computed for the soil under investigation throughout the frequency spectrum as it is frequency-dependent. From Equations (4.1) to (4.4) in Chapter 4 and from the calibration result, the important values for shear modulus calculation have been determined and summarized in Tables 6-1 and 6-2, where f_n – resonant frequency of the calibration bar; ω

-natural circular frequency of vibration of the sample. With the help of that, the shear modulus ratio for the RC test will be derived for each strain value.

TABLE 6-1. Calibration results

		f_n**(Hz)**	ω^***(rad/s)**	ω^2 **(rad/s)²**	$1/\omega^2$**(1/rad²)**	**Intercept**
15 mm bar	Top plate	73.5	461.814	213272.3	4.689	
	Weight #1	72.1	453.017	205225	4.873	
	Weight #2	71.2	447.362	200133.5	4.997	
	Weight #3	70.6	443.592	196774.6	5.082	**-0.00400908**
12.5 mm bar	Top plate	52.2	327.983	107572.4	9.296	
	Weight #1	51.5	323.584	104706.6	9.55	
	Weight #2	50.2	315.416	99487.2	1.055	
	Weight #3	50.1	314.788	99091.2	1.009	**-0.00337053**
10 mm bar	Top plate	33.8	212.372	45101.7	2.217	
	Weight #1	33.3	209.231	43777.2	2.284	
	Weight #2	32.8	206.088	42472.5	2.354	
	Weight #3	32.4	203.575	41442.9	2.413	**-0.00384692**
Average						**-0.00374218**

TABLE 6-2. Computed values for determining the shear modulus

Parameter	Value
I_0	-0.003742178
I	0.00042875
I/I_0	-0.114571642
β	0.10469
Dry Bulk density (ρ, Mg/m^3)	1.4

6.2. Resonant Column (RC) Test

The main idea behind RC testing is to vibrate the cylindrical soil specimen in its fundamental oscillation mode while accurately measuring the resonance frequency (Dammala, 2019) and its amplitude (Figure 6.2). This work used RCT to assess the changing dynamics of well-graded sand with silt under confining pressures (σ_c) of 50, 100, 150, and 200 kPa. Accurate assessment of dynamic soil parameters over various strain magnitudes and σ_c was made possible by the fixed-free configuration of the RCA. Figure 6.3 displays a usual resonant frequency chart produced during testing, emphasizing the soil's responsiveness and resonance properties under controlled circumstances.

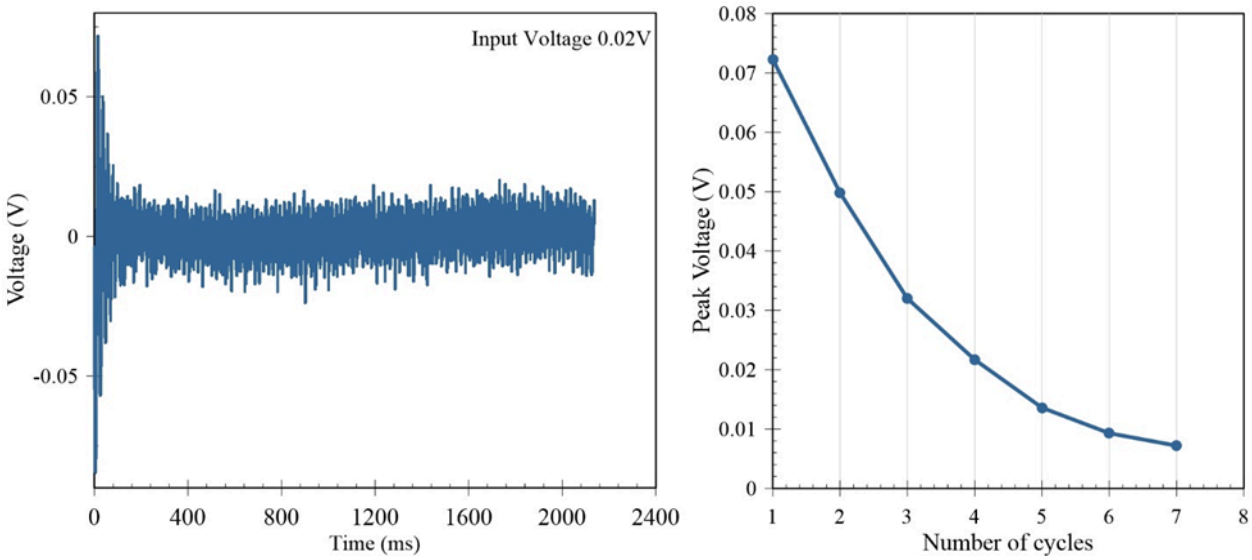

Figure 6.2. A typical illustration of damping ratio testing

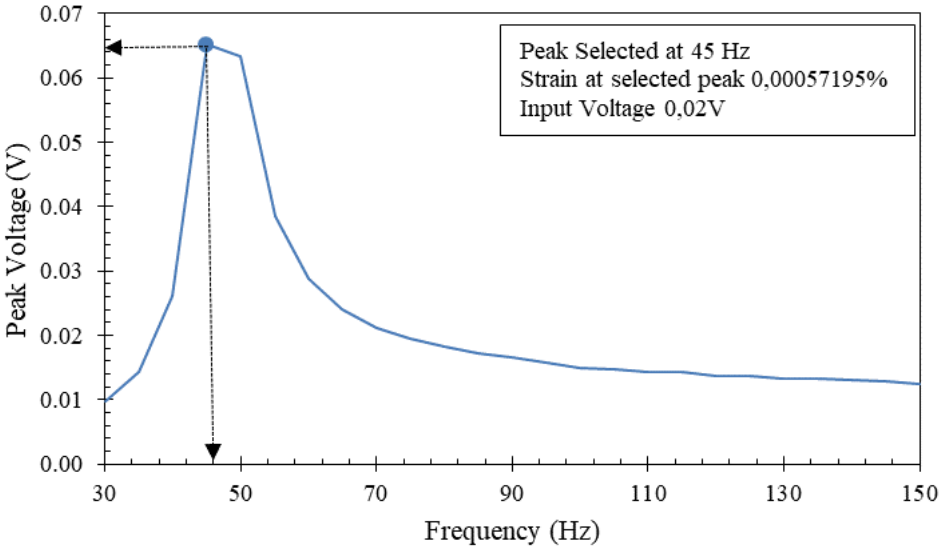

Figure 6.3. A typical illustration of the resonance frequency for a particular shear strain magnitude

6.2.1. Shear modulus vs. shear strain (G vs. γ)

The correlation between shear strain and shear modulus (G) under various confining pressures is shown in Fig. 6.4. The findings demonstrate that the shear modulus falls with increasing shear strain amplitude, suggesting a drop in soil elasticity. The non-linear nature of soil under dynamic loading circumstances is reflected in the decreasing effect of confining pressure on sample stiffness at greater strain levels.

The outcomes show a notable rise in shear modulus ratios at smaller strain estimates, underscoring the crucial function of confining pressure. Denser grain packing is encouraged by higher confining pressures, increasing the elasticity and shear stiffness of the material (Adari et al., 2023). This tendency is pronounced at deeper levels, where a more compact soil matrix leads to bigger dynamic G values.

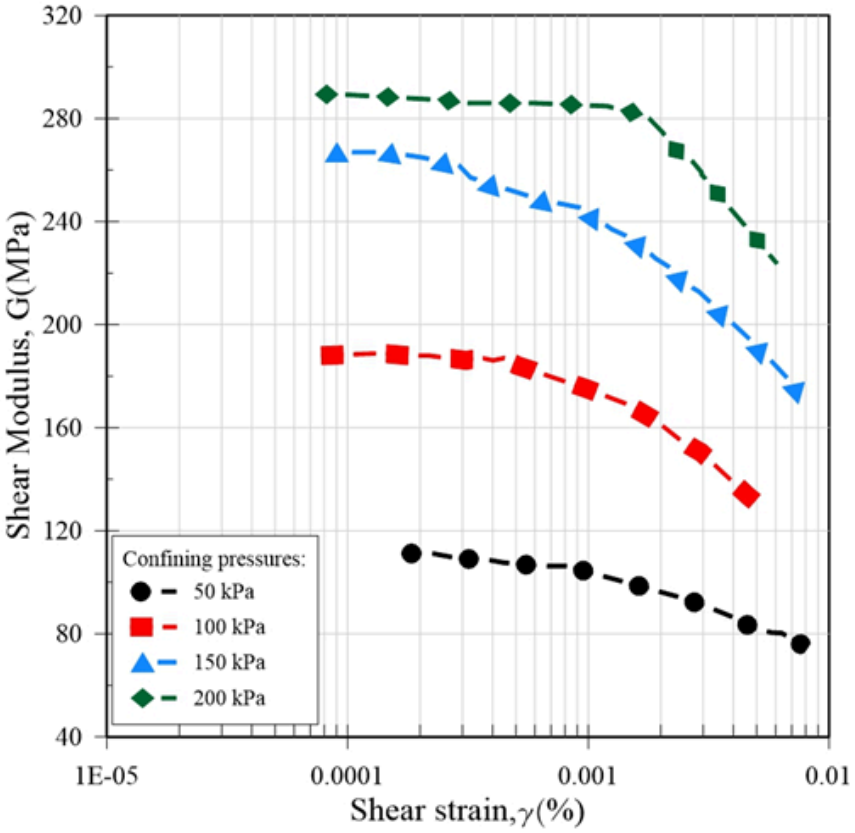

Figure 6.4. G vs. γ for different σ_c (for RC tests)

6.2.2. Damping ratio vs. shear strain (D vs. γ)

According to ASTM guidelines (2015), the damping ratio (D) of the specimen was calculated using the free vibration decay technique. An accelerometer on the RC drive panel measured the soil sample's reaction. The excitation was stopped during testing, and the decay of free vibrations brought on by sinusoidal stimulus was noted.

The decay curve was estimated using the logarithmic decrement technique, where the trend of the best-fit line represents the logarithmic decrement. The method calculated the damping ratio using 10 vibration cycles, as shown in Figure 6.5 (GDS Resonant Column 2010).

The damping ratio values were calculated using Equations (4.5) and (4.6) in Chapter 4.

Figure 6.5 illustrates the rising concave trend of the damping ratio as it rises with shear strain. Adari et al. (2023) explain this by a rise in energy loss linked to larger cyclic loading amplitudes. Interestingly, changes in confining pressure do not affect the damping ratio throughout the observed strain range, suggesting that the intrinsic material characteristics are

stable. At greater strain levels, however, higher confining pressures are linked to a modest drop in the damping ratio, possibly due to improved particle contact and less dissipated energy.

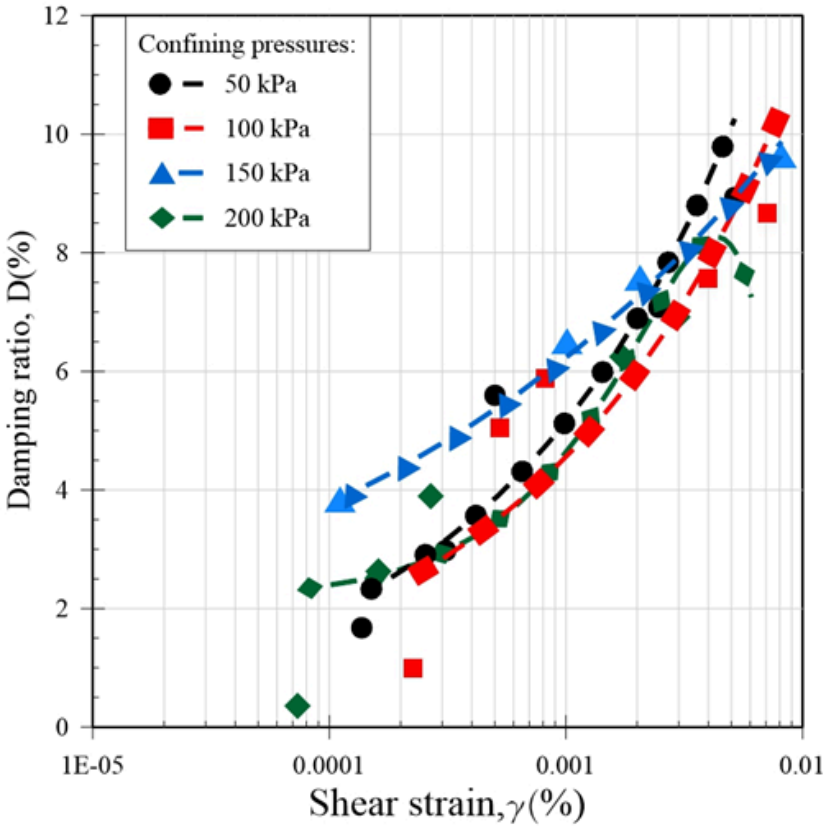

Figure 6.5. D vs. γ for different σ_c (for RC tests)

6.3. Cyclic Torsional Shear Testing

The material was subjected to CTS tests employing the same resonant column equipment at an amount of σ_c 50 kPa- 200 kPa to examine the effects of low-energy cyclic loading. Each test was conducted one after the other. The coils were run at the smallest voltage possible for the first CTS testing, resulting in a strain amplitude of about 0.01% (Sakshi and Sebastian 2023). The excited voltage was gradually raised in the following tests at every confining pressure to reach a strain intensity of 1%.

6.3.1. Shear modulus vs. shear strain (G vs. γ)

Figure 6.6 shows the correlation between shear modulus (G) and shear strain as determined by the CTS test. The effect of σ_c on the G is insignificant at higher stresses (more

than 0.1%). Because CTS testing uses a gradual, quasi-static load as opposed to RCT, strain amplitudes greater than RC tests are possible.

The findings show that the shear modulus values (G) were decreased during the first loading phases, and while the strain parameters grew, they showed an upward curve pattern. This trend emphasizes how soil stiffness gradually decreases with increasing strain amplitudes, independent of confining pressure.

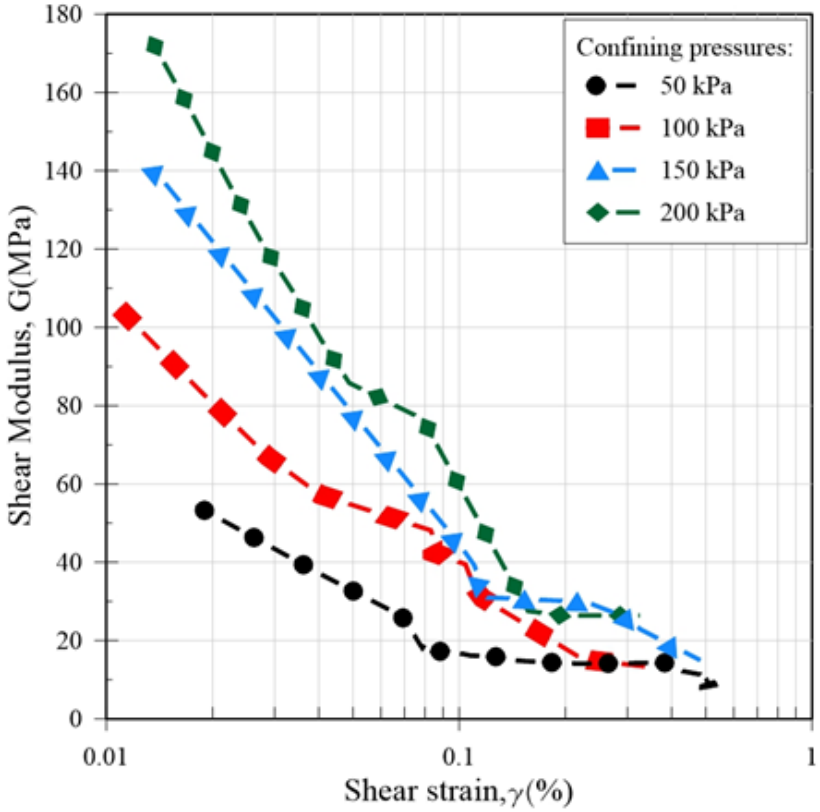

Figure 6.6. G vs. γ for different σ_c (for CTS tests)

6.3.2. Damping ratio vs. shear strain (D vs. γ)

As determined by CTS investigation, increased shear strain magnitudes are consistently associated with increased damping ratios (D). At lower strain stages, this pattern, which is seen in Figure 6.7, has a curved upward behavior that progressively lessens at higher strain values. Curiously, the damping rates (D) seem to somewhat reduce as σ_c rises, especially at greater strain magnitudes. Confining pressure less impacts the damping ratio at a strain value of about 0.1%. During greater confining pressures, when particle contact gets more restricted, this

behavior represents the well-graded sand's decreased potential to dissipate energy (Adari et al., 2023).

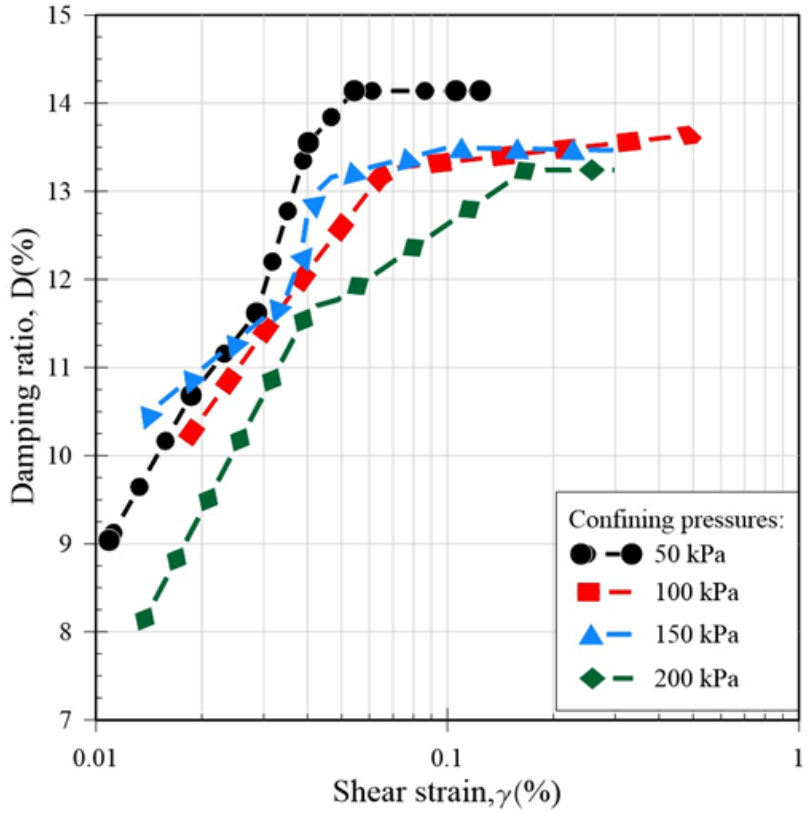

Figure 6.7. D vs. γ for different σ_c (for CTS tests)

6.3.3. Impacts of Shearing Strain

The behavior of well-graded sand with silt is shown in Figure 6.8 over a range of loading cycle counts: N=1, 10, 100, 1000. It was tested during cyclic torsional shear (CTS) test at a confining pressure of 150 kPa. The amplitudes of strain produced throughout examination are represented by the following numbers: $\Delta\gamma$ = 0.06, 0.1, 0.16, and 0.22%. The development of soil properties in longer cycles is impacted by such strain stages, which correlate to various stress amplitudes.

Despite reaching 1000 cycles, the material shows a virtually elastic behavior at relatively small magnitudes ($\Delta\gamma$ = 0.06%), with only minor modifications in loop form. Nevertheless, the loops exhibit notable asymmetry and enlargement at greater strain values ($\Delta\gamma$ =0.22%), suggesting enhanced distortion, particle modification, and possible elongation impacts.

The change from convex (oval-shaped form) to concave loops of hysteresis illustrates the strain-dependent irregularity of the sample, in which cyclic loading causes a growing loss of stiffness and more significant power loss. In the initial periods (N = 1 and N = 10), the loops retain a more dense and rigid shape, while at N = 100 and N = 1000, they transform toward a primarily concave and extended appearance.

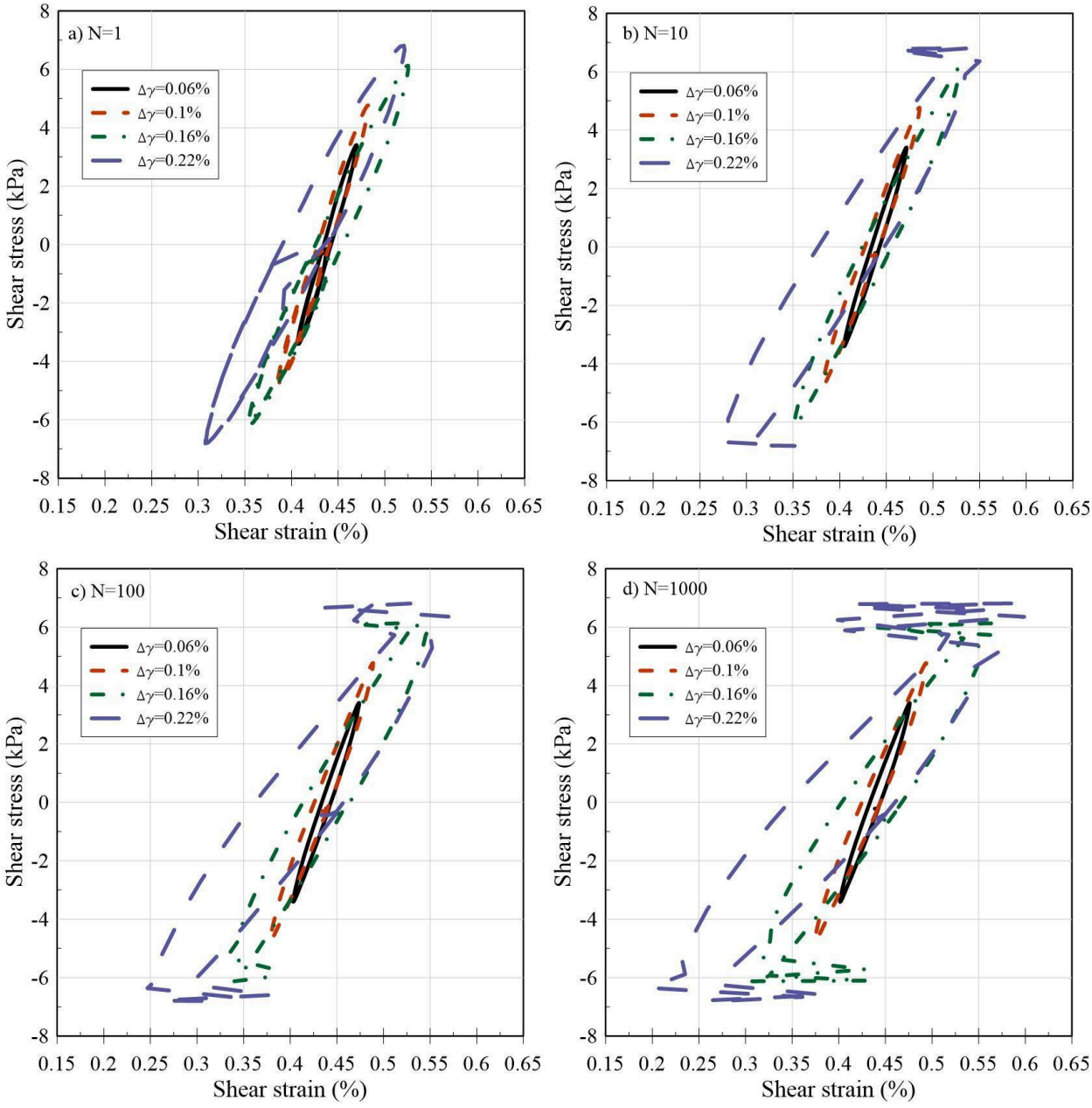

Figure 6.8. Hysteretic response of the sample at different loading cycles

The deterioration of shear modulus (G) due to growing shear strain is shown in Figure 6.6, and the hysteresis loops of the exact sample at various strain amplitudes and periods of

loading at 150 kPa σ_c are captured in Figure 6.8. Both of these illustrations show a good association. CTS testing at gradually rising strain magnitudes, comprising the numbers shown in Figure 6.8, yielded the shear modulus measurements shown in Figure 6.6.

The strain-dependent smoothing pattern of the material is confirmed by the patterns seen in loop enlargement and stiffness decrease, enhancing its significance in seismic evaluation and construction of foundations under cyclic loading circumstances.

6.3.4. Impacts of Loading cycles

The hysteretic behavior of the tested sample under CTS testing at a confining pressure of 150 kPa is shown in Figure 6.9. This behavior was noted at several input voltages from 0.5V to 1V. As input voltage rises, the shear stress-strain loops exhibit a noticeable rising pattern, with greater slopes within the first phases. The loops unevenly grow with increasing voltage and strain levels, indicating a slow shift onto more nonlinear soil dynamics. At higher voltages (0.8V, 0.9V, and 1V), the difference is very noticeable, suggesting that the underlying structure of the soil has changed significantly in response to higher shear loads and more cycles. The loops' asymmetry and extension imply that greater strain amplitudes cause component rearrangement, which changes the soil structure from tight to more scattered.

Figure 6.9 shows how the soil reacts to rising strain amplitudes brought on by higher input voltages, in contrast to Figure 6.8, in which loop development is caused through increased loading periods (N) at a fixed strain amplitude. As strain builds up over several cycles, the loops in Figure 6.8 progressively change form from convex to concave as N increases. This change indicates an impairment of initial stiffness as well as increasing deformation. On the other hand, Figure 6.9 shows how broader and more unequal loops, which indicate nonlinear dynamics and increased energy loss, are quickly produced by higher input voltages.

The discovered asymmetrical hysteresis loops are consistent with earlier research on sandy soils that found complicated, nonlinear soil reactions with unique stress-strain routes under high-strain dynamic situations, such as those brought on by excessive input voltages (Kumar et al., 2017). Continuous high-strain cycles lead to increased curvature and a possible decrease in security, as seen by the growing imbalance and loop extension with strain.

Departures from a perfect elliptical form, where strain distribution and energy loss cause unequal stress-strain behavior, are called asymmetry of loops. These features highlight how crucial it is to

faithfully model soil behavior under extreme strain circumstances when dynamic parameters like elasticity and damping necessitate careful assessment.

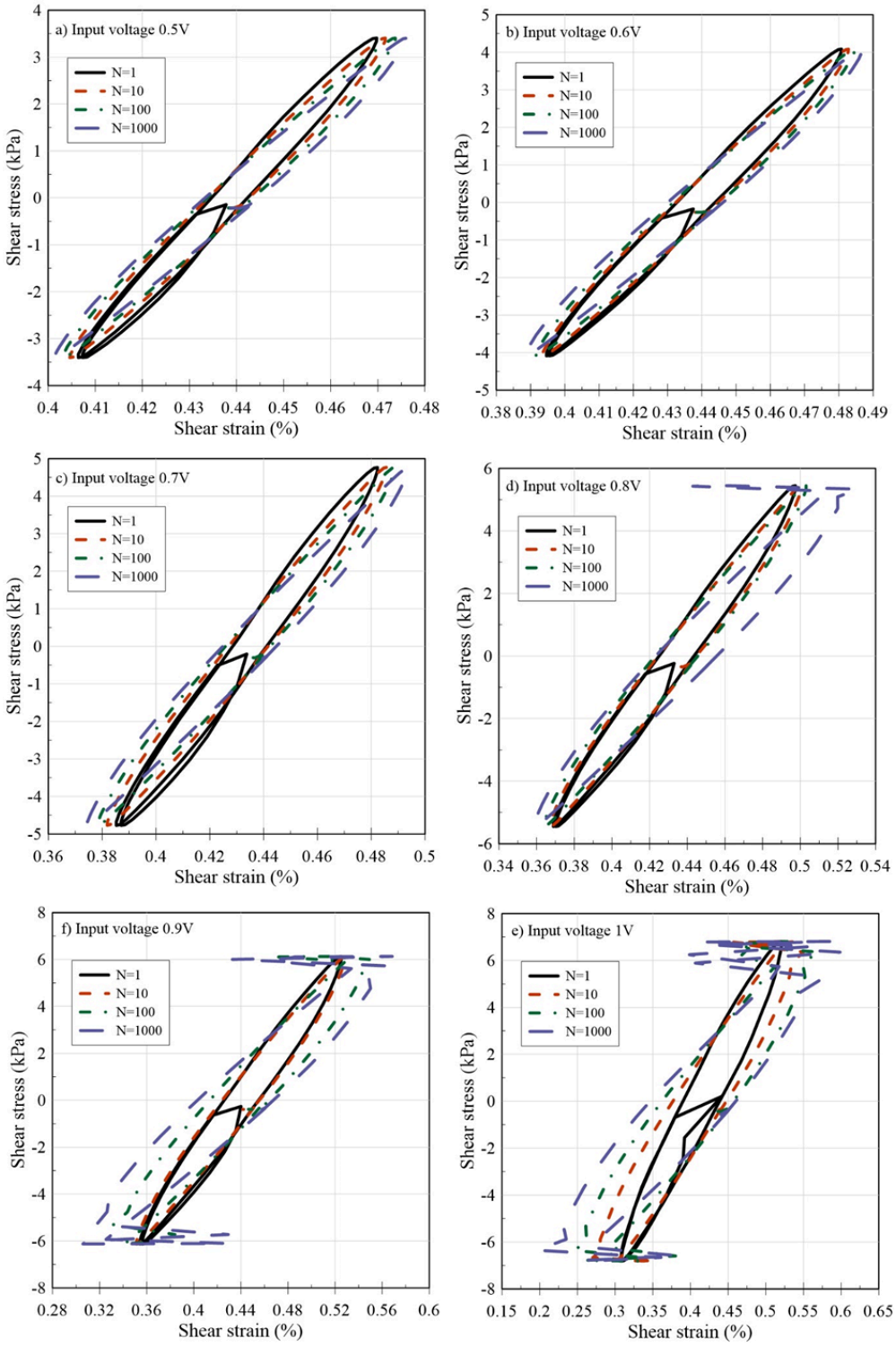

Figure 6.9. Hysteretic response of the sample at different voltages

6.4. Normalized shear modulus (G/G_{max} vs. γ)

The connection among normalized shear modulus (G/G_{max}) and shear strain (γ) for silt-containing well-graded sand evaluated at confining pressures of 50, 100, 150, and 200 kPa is shown in Figure 6.10. Based on the testing technique used, the data is divided into two different regions: the cyclic torsional shear (CTS) test, which goes beyond 0.01%, and the resonant column (RC) test, which catches the low-strain range between 10^{-5}% and 0.01%. While the CTS test shows a steady decrease in stiffness at increasing strain levels, the RC test offers important information regarding soil behavior in the low-strain region, where stiffness stays relatively high.

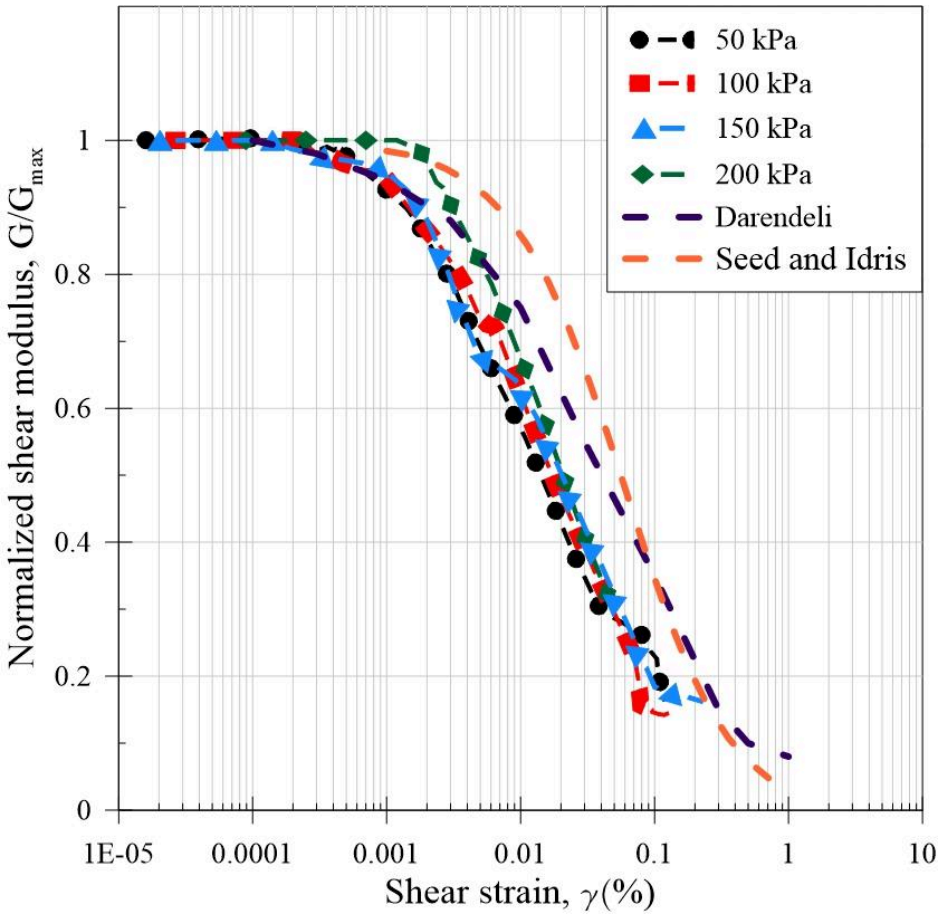

Figure 6.10. G/G_{max} vs. γ

There is little change in the normalized shear modulus at various confining pressures in the low-strain region (up to around 0.001%). This uniformity shows how the sample retains stiffness within its elasticity range. However, a progressive decrease in G/G_{max} is noticeable when strain rises into the range of intermediate values (going from 0.001% to 0.1%), indicating the start of soil softening.

The decline in G/G_{max} is more noticeable at greater strain levels (above 0.1%), and modulus values exhibit a dramatic drop. This pattern closely resembles the reference curve for strain-dependent modulus performance that Darendeli (2001) suggested for silt-containing well-graded sand, as well as the Seed and Idris(1970) model for sandy soils. The Darendeli model accurately depicts the stiff deterioration of well-graded sand with silt under a range of confining pressures, as evidenced by the alignment of the experimental results with the model.

This comparison highlights how, as strain levels rise, well-graded sand with silt changes from an initially elastic to a progressively plastic reaction. The work offers a thorough knowledge of how well-graded sand with silt rigidity changes across a broad range of strain levels by documenting these transitions, which is beneficial for geotechnical applications, including foundation stability evaluations and earthquake design.

6.5. Damping ratio (D vs. γ)

The connection between RC and CTS tests for damping ratio tested for different confining pressures is shown in Figure 6.11. As it can be seen, the damping ratio values range from 0 to 16%. As shear strain increases, the damping ratio increases for all confining pressures, which shows typical nonlinear behavior of the soils. While higher confining pressures tend to slightly reduce damping at low strains, the differences diminish at higher strain levels, where the curves begin to converge.

The graph depicts soil behavior across a broad strain range using data from both cyclic torsional shear and resonant column tests. The cyclic torsional shear test extends into medium to large strains, while the resonant column covers the small-strain region. For the purpose of simulating seismic soil response, this combined approach offers a thorough understanding of how soil damping changes as strain increases.

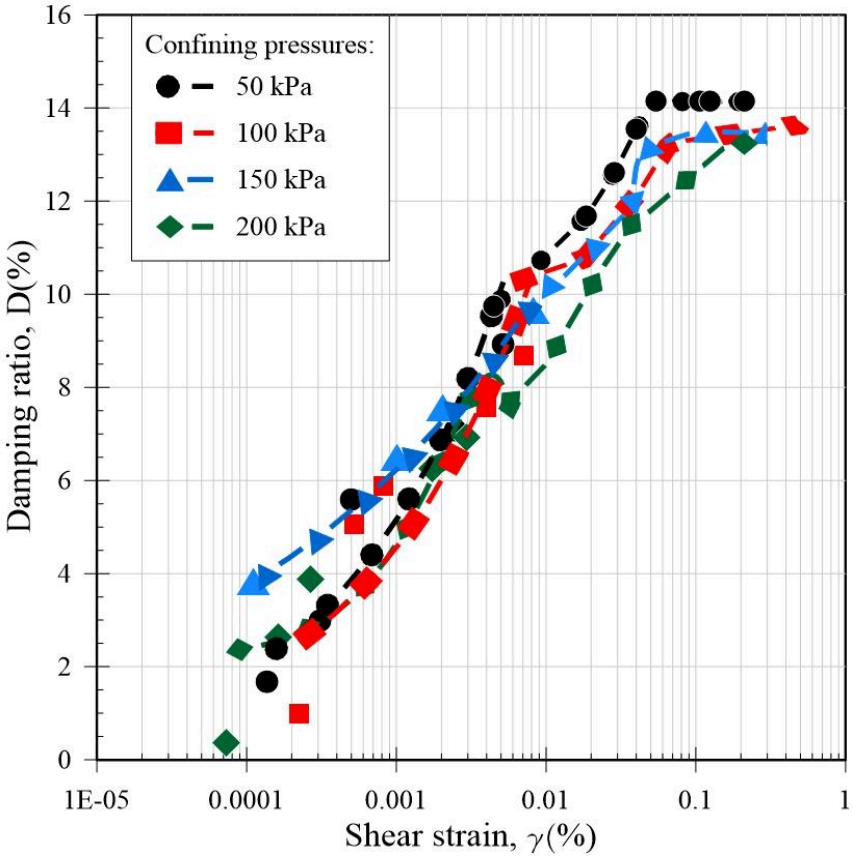

Figure 6.11. D vs. γ

Chapter 7. Conclusion

This study used resonant column and cyclic torsional shear experiments to evaluate the dynamic characteristics of well-graded sand with silt. Shear modulus, damping ratio, and modulus reduction curve are the three primary components of dynamic soil characteristics. These characteristics are evaluated on well-graded sand with silt specimens from Astana at various relative densities in small-to-intermediate strain range values. For those tests, the most suitable apparatus is the resonant column apparatus, which has already been installed in our laboratory.

The most significant and often utilized dynamic soil parameters in soil dynamic issues and ground reaction analysis are cyclic shear strength, shear modulus, and damping ratio; yet, there is a lack of complete laboratory data on regional soils. To shed light on the most often used model parameters, a thorough literature analysis on the modeling of soil small strain stiffness has already been provided. Additionally, the investigation of correlation-based model parameter determination has been done. Furthermore, a description of the fundamental ideas behind dynamic soil properties, their measurement, and their dynamic soil characteristics was given.

The combined results of the cyclic torsional shear (CTS) and resonant column (RC) tests offer important new information on how well-graded sand with silt behaves under different confining pressures in terms of strain. These findings advance our knowledge of the mechanical characteristics of silt-containing well-graded sand and how it behaves under dynamic loading circumstances.

- According to the results of the RC test, silt-graded sand retains its high stiffness at extremely low stresses while reducing its shear modulus very little at various confining pressures. This suggests that silt-graded sand maintains its elastic properties effectively in shallow or low-strain settings. A progressive decrease in shear modulus is noted as strain levels rise, indicating the beginning of material softening. This pattern, which holds for all confining pressures, emphasizes how well-graded sand with silt loses elasticity as strain rises.
- According to the Darendeli (2001) theory of well-graded sand with silt, the CTS test results show a more noticeable drop in rigidity at higher strain values.
- Hysteresis loops shown during CTS testing change from convex to concave geometries with greater loading cycles, confirming the model's accuracy in representing high-strain performance for this soil type. Internal structural

alterations, such as particle arrangement and larger void spaces, are reflected in this transformation. These changes lead to a loss of resilience and an increased risk of deformation under cyclic loading.

- The findings highlight how crucial it is to consider confining pressures and strain levels when assessing the mechanical characteristics of silt-containing well-graded sand. Their relevance in engineering practices, especially in seismic risk assessments and foundation construction, where comprehending the impacts of cyclic loading is crucial, is supported by their strong connection with prediction models such as Darendeli (2001).

The study improves our knowledge of the dynamic soil characteristics of Astana's silt-and-sand well-graded sand, providing important information for the region's infrastructure development and seismic hazard assessment. More research is required to develop prediction models and broaden their application under a variety of geotechnical circumstances to expand on these results and enhance resilience to urban environments in high-risk areas. To increase the range of their practical applications, future studies should investigate the application of these discoveries to different varieties of soil in the Republic of Kazakhstan, along with various environmental circumstances, such as fluctuating temperatures and moisture levels.

References

Abdialim, S., Hakimov, F., Kim, J., Ku, T., and Moon, S.W*., (2021) Seismic Site Classification from HVSR Data using the Rayleigh wave ellipticity inversion: A case study in Singapore, Earthquake and Structures, 21(3)

Alshembari, R., Parolai, S., Boxberger, T., Sandron, D., Pilz, M., & Sylacheva, N. (2020). Seasonality in site response: An example from two historical earthquakes in Kazakhstan. *Seismological Research Letters, 91*(1), 415–426. https://doi.org/10.1785/0220190114

Amey, R.M.J., Elliott, J.R., Hussain, E., Walker, R., Pagani, M., Silva, V., Abdrakhmatov, K.E. and Watson, C.S. (2021). Significant Seismic Risk Potential From Buried Faults Beneath Almaty City, Kazakhstan, Revealed From High‐Resolution Satellite DEMs. *Earth and Space Science*, 8(9). doi:https://doi.org/10.1029/2021ea001664

ASTM D4015–15 (2015), "Standard test methods for modulus and damping of soils by resonant-column method", *ASTM International*, West Conshohocken, PA

Bondár, I., Storchak, D. (2011). Improved location procedures at the International Seismological Centre.*Geophys. J. Int.,*186,1220–1244

Botabekova, Sh. B., Shorin, O. A., & Yurchenko, T. A. (2021). Report on engineering and geological surveys on the object: "Construction of a plant of thermal insulation materials in Talgar district of Almaty region" [Review of Report on engineering and geological surveys on the object: "Construction of a plant of thermal insulation materials in Talgar district of Almaty region"]. "Almaty Building Research" LLP.

Bharat bhushan prasad. (2011). *Fundamentals of soil dynamics and earthquake engineering*. PHI Learning Pvt. Ltd. Chapter 6, 292-353

Das, B. M., & Luo, Z. (2016). Principles of Soil Dynamics. Cengage Learning.

Darendeli, M. B. (2001).Development of a new family of normalized modulus reduction and material damping curves (Ph.D. dissertation). University of Texas at Austin.

Dutta, T. T. (2015). Dynamic Properties of Clean Sand and Expansive Clay from Resonant Column Studies [Dissertation]. Indian Institute of Technology Hyderabad

Flores-Guzmán M, Ovando-Shelley E, Valle-Molina C (2014). Small-strain dynamic characterization of clayey soil from the Texcoco Lake, Mexico. *Soil Dyn Earthq Eng*. 63:1–7.

GDS Resonant Column, 2010. The GDS Resonant Column System Handbook

Hardin, B., & Drnevich, V. (1972). Shear modulus and damping in soils: Design equations and curves. In Journal of the Soil Mechanics and Foundations Division, ASCE 98(SM7) (pp. 667-692). https://trid.trb.org/view.aspx?id=126413.

Hoque, M. M. (2016). Evaluation of Dynamic Properties of a Sandy Soil Using Cyclic Triaxial Test [Thesis Evaluation of Dynamic Properties of a Sandy Soil Using Cyclic Triaxial Test].

Henni, P.H.O., Fyfe, C.J., Marrow, P.C. (1998). The BGS World Seismicity Database; Technical Report WL/98/13; BGS: Nottingham, UK.

INFORM.KZ (2023). Up to 30% of Almaty buildings may collapse in case of a strong quake, Emergency Ministry. [online] Казинформ. Available at: https://www.inform.kz/en/up-to-30-ofalmaty-buildings-may-collapse-in-case-of-strong-quake-emergency-ministry_a4039182 [Accessed 4 September. 2023]

Ishihara, K., Sodekawa, M. and Tanaka, Y. (1978). Effects of over consolidation on liquefaction characteristics of sands containing fines. *Dynamic Geotechnical Testing,ASTM STP 654*, 246–264.

Johann Facciorusso. (2020). An archive of data from resonant column and cyclic torsional shear tests performed on Italian clays. *Earthquake Spectra*, *37*(1), 545–562. https://doi.org/10.1177/8755293020936692

Kramer, S.L. (1996). *Geotechnical earthquake engineering*. Pearson Education India

Kumar, S., & Murali K., Arindam., A. & Dey, (2013). Parameters Influencing Dynamic Soil Properties: A Review Treatise.

Luna, R., and Jadi, H., (2000).“Determination of dynamic soil properties using Geophysical methods,” Department of Civil Engineering, University of Missouri-Rolla.

Mahinroosta, R., and Oshtaghi, V. (2021), "The effect of particle shape on the deformation and stress reduction of a gravel soil due to wetting", Scientific Reports, 11(1). https://doi.org/10.1038/s41598-021-95731-y

Moon, S.W*., Mukhtarkhan, D., Khamitov, R., Abdialim, S., Y., Khomyakov, Kim, J., and Ku, T., (2024) "Liquefaction Assessment using Surface Waves in Kazakhstan", 18th World Conference on Earthquake Engineering (WCEE2024), June 30 – July 5, 2024, Milan, Italy.

Oztoprak, S., & Bolton, M. (2013). Stiffness of sands through a laboratory test database. *In Géotechnique 63 No1* (pp. 54-70). https://doi.org/10.1680/geot.10.P.078.

Paiyz, N., Khoschanova, K., Abdialim, S., & Moon, S.-W. (2024, August 22). Dynamic properties of silty sand. https://www.researchgate.net/publication/385084583_Dynamic_properties_of_silty_sand

Rashid, M.S., Zhang, D., Moon, S.-W., Sarkulova, D., Shokbarov, Y., Kim, J. (2023). Macro-Seismic Assessment for Residential Buildings Constructed in the Soviet Union Era in Almaty, *Kazakhstan Buildings*,13, 1053. https://doi.org/10.3390/buildings13041053

Rashid, S. M., Zhang, D., **Moon, S.W.**, Shokbarov, Y., Kim, J., (2024) Analytical Seismic Assessment for Reinforced Concrete Moment Frame Residential Buildings Constructed in the Soviet Union Era in Almaty, Kazakhstan, *Bulletin of Earthquake Engineering.*

Sagidullina N, Satyanaga A, Kim J and Moon S-W (2025). Engineering behavior and geotechnical challenges of sulfate-rich soils in Astana. *Front. Built Environ*. 10:1504643. doi: 10.3389/fbuil.2024.1504643

Sakshi Rohilla, & Sebastian, R. (2023). Resonant column and cyclic torsional shear tests on Sutlej river sand subjected to the seismicity of Himalayan and Shivalik hill ranges: A

case study. *Soil Dynamics and Earthquake Engineering*, 166, 107766–107766. https://doi.org/10.1016/j.soildyn.2023.107766

Sas, W., Gabryś, K., & Szymański, A. (2017). Experimental studies of dynamic properties of Quaternary clayey soils. *Soil Dynamics and Earthquake Engineering*, *95*, 29–39. https://doi.org/10.1016/j.soildyn.2017.01.031

Seed, H.B. and Idriss, I.M. (1970). "Soil Moduli and Damping factors for dynamic response analyses", EERC/70-10, College of Engineering university of California, Berkeley

Shankar S.,(2013). "Parameters Influencing dynamic Soil Properties," *International Journal of Innovative Research in Science, Engineering and Technology*., v 03, pp.47-60

Shinde, N.S., and Kumar, J. (2021), "Calibration exercise of fixed-free resonant column apparatus", in: T.G. Sitharam, S.V. Dinesh, R. Jakka (eds), Soil Dynamics, Lecture Notes in Civil Engineering, vol 119, Springer, Singapore. https://doi.org/10.1007/978-981-33-4001-5_4

Silacheva, N.; Kulbayeva, U.; Kravchenko, N. (2018). Probabilistic seismic hazard assessment of Kazakhstan and Almaty city in peakground accelerations.*Geodesy Geodyn.,*9, 131–141

Silver, M.L., Tatsuoka, F., Phukunhaphan, A. and Avramidis, A.S. (1980). Cyclic undrained strength of sand by triaxial test and simple shear test. *Proceedings of 7th World Conference on Earthquake Engineering,* Istanbul, Vol. 3, 281–288.

Sitharam, T. G., Dinesh, S. V., & Ravi Jakka. (2021). *Soil Dynamics*. *Springer Nature*. Chapter 2

Stokoe KH II, Darendeli MB, Andrus RD, Brown LT (1999). Dynamic soil properties: laboratory, field and correlation studies, theme lecture. *In: Proceedings of the second international conference earthquake geotechnical engineering, Vol. 3*,Lisbon, Portugal,p.811–45.

Szilvágyi, Z. (2018). Dynamic Soil Properties of Danube Sands (pp. 23–26) [PhD Dissertation Dynamic Soil Properties of Danube Sands].

Tatsuoka, F., Iwasaki, T., & Takagi, Y. (1978). Histeretic damping of sand under cyclic loading and its relation to shear modulus. In Soils and Foundations Vol 18(2) (pp. 25-40). Japanese Society of Soil Mechanics and Foundation Engineering https://doi.org/10.3208/sandf1972.18.2_25 .

Tectonic Structures. Available online: http://activetectonics.la.asu.edu/N_tien_shan/N_tien_shan.html (accessed on 5 October 2023).

Vucetic, M., & Dobry, R. (1991). Effect of soil plasticity on cyclic response. *In Journal of Geotechnical Engineering, ASCE,* Vol 117 (pp. 89-107). https://doi.org/10.1061/(ASCE)0733-9410(1991)117:1(89).

Wong, R.T., Seed, H.B. and Chan, C.K., (1975). Cyclic loading liquefaction of gravelly soils. *Journal of Geotechnical Engineering, ASCE,* Vol.101, No.GT6, pp. 571–583

Wong, J. K. H., Wong, S. Y., & Wong, K. Y. (2021). Extended model of shear modulus reduction for cohesive soils. Acta Geotechnica. https://doi.org/10.1007/s11440-021-01398-0

Zhanabayeva, A., Moon, S.W*., Ocheme, J. I., Yeraly, S., Khomyakov, V.A., Kim, J., Satyanaga, A., (2023) Comparative analysis of seismic design codes adhering to the Kazakhstani and European approaches, Sustainability, 15, 615, https://doi.org/10.3390/su15010615